A role for the locus coeruleus in the modulation of feeding

Natale R. Sciolino[1], Christopher M. Mazzone[1], Nicholas W. Plummer[1], Irina Evsyukova[1], Jaisal Amin[1], Kathleen G. Smith[1], Christopher A. McGee[2], Sydney A. Fry[1], Cindy X. Yang[1], Jeanne M. Powell[1], Michael R. Bruchas[3], Alexxai V. Kravitz[4], Jesse D. Cushman[1], Michael J. Krashes[5], Guohong Cui[1], Patricia Jensen[1]*.

[1]Neurobiology Laboratory, National Institute of Environmental Health Sciences, National Institutes of Health, Dept. of Health and Human Services, Research Triangle Park, NC, USA.

[2]Comparative Medicine, National Institute of Environmental Health Sciences, National Institutes of Health, Department of Health and Human Services, Research Triangle Park, NC, USA.

[3]Departments of Anesthesiology and Pharmacology, Center for the Neurobiology of Addiction, Pain, and Emotion, University of Washington, Seattle, WA, USA.

[4]Department of Psychiatry, Washington University, St Louis, MI, USA.

[5]National Institute of Diabetes and Digestive and Kidney Diseases, National Institutes of Health, Dept. of Health and Human Services, Bethesda, MD, USA.

Correspondence to:

*Patricia Jensen, Ph.D.

Neurobiology Laboratory

National Institute of Environmental Health Sciences

111 T.W. Alexander Drive

Bldg. 101, Rm. F118 (Mail Drop F1-11)

Research Triangle Park, NC 27709

Tel.: 984-287-3413

email: patricia.jensen@nih.gov

SUMMARY: Noradrenergic neurons of the locus coeruleus (LC-NE) are known to play an important role in arousal, emotion, memory and cognition. In the present study, we use fiber photometry combined with chemogenetic and optogenetic approaches to demonstrate a previously unrecognized role for LC-NE neurons in the modulation of feeding. We show that endogenous activity of LC-NE neurons is enhanced while approaching food and suppressed during feeding. These changes in LC activity during feeding behavior are attenuated as mice approach satiety, demonstrating that nutritional state modulates LC responses to food. Direct activation of LC-NE neurons results in the suppression of feeding. Further, activation of an LC projection to the lateral hypothalamus also suppresses feeding. Together, these findings demonstrate a direct causal role for LC-NE activity in the modulation of feeding.

KEYWORDS: locus coeruleus, norepinephrine, feeding, metabolism, photometry, lateral hypothalamus, optogenetics, chemogenetics, anxiety, and aversion.

INTRODUCTION

Evidence that noradrenergic neurons of the locus coeruleus (LC-NE) play a role in arousal was first established in a series of electrophysiology experiments conducted over four decades ago. These studies consistently showed that LC neurons in several different species are phasically activated during high-arousal behavioral states (e.g., orienting, waking, startle) and in response to salient sensory stimuli[1-5] (reviewed in [6,7-9]). More recent studies using opto- and chemogenetic approaches have demonstrated that LC-NE activity is both necessary and sufficient for promoting behavioral arousal, including sleep-to-wake transitions and emergence from anesthesia[10,11].

In contrast, much less is known about the contribution of LC-NE activity to low-arousal behavioral states (e.g. sleeping, grooming, feeding). One early electrophysiology study noted that LC-NE activity is transiently decreased in rats during sleeping, grooming, and drinking a sucrose reward[2]. In a second study, decreased LC activity was observed in two monkeys eating apples[12]. While these observations suggest that LC-NE activity may play a role in modulating feeding, this possibility has not previously been tested. In the present study, we used fiber photometry combined with chemogenetic and optogenetic approaches to test the hypothesis that activity of LC-NE neurons is involved in the modulation of feeding.

RESULTS

To identify the natural activity patterns of LC-NE neurons during feeding behavior, we used fiber photometry to monitor fluorescence of the calcium sensor GCaMP6f in LC-NE neurons. We selectively target these neurons by co-injecting Flp-dependent GCaMP6f and tdTomato AAVs into the LC of *Dbh*^{Flpo} mice (LC$^{GCaMP/tdT}$) **(Fig. 1a)**. To control for changes in fluorescence due to movement, GCaMP6f signal was normalized to tdTomato to yield a fluorescent ratio using a spectral unmixing approach[13]. To verify our recording conditions were sensitive to detect LC activity, we presented mice a visual flash known to activate LC

neurons[2,14]. We observed the expected increase in LC-NE activity in response to the visual stimulus **(Supplementary Fig. 1)**, validating that we can reliably detect changes in LC-NE activity in the behaving mouse.

To determine if LC activity is altered during feeding-related behaviors, $LC^{GCaMP/tdT}$ mice were fasted overnight and photometry recordings were collected during a 1-hr session while mice approached and consumed food pellets from the feeding experimentation device (FED)[15] **(Fig. 1a)**. To minimize the effects of stress and novelty during the experiments, mice were habituated for several days to eat from the FED while in the testing arena. To determine if nutritional status influences LC responses during approach and consumption, we compared LC activity early and late in the session as mice approached satiety. Assessment of approach revealed an increase in activity of LC-NE neurons during approach early in the session. This approach-related LC response was abolished later in the session when mice had consumed more food **(Fig. 1b-e)**, suggesting that energy levels modulate LC activity during appetitive behavior.

Assessment of consummatory responses revealed that LC-NE activity was rapidly suppressed during feeding **(Fig. 1b-d)**. This decrease in LC activity was observed during consumption of pellets throughout the session **(Fig. 1d)**. To determine if the transition from hunger to satiety had a gradual impact on food-related LC activity across the trial, we next performed a linear regression analysis. We found the suppression of LC-NE activity during feeding was significantly attenuated as fasted mice ate more within the trial (R^2=0.049) **(Fig. 1e),** suggesting energy levels gradually modulate LC activity during consumption. Importantly, there was no significant change in baseline LC-NE activity **(Supplementary Fig. 2)** or movement velocity **(Supplementary Fig. 3**) as mice consumed more pellets across the session. Taken together, these findings suggest nutritional state-related changes in LC-NE activity during feeding-related behavior was not driven by alterations in movement.

To determine whether activation of LC-NE neurons would directly influence feeding behavior, we employed an intersectional chemogenetic approach in which the excitatory Gq-coupled receptor hM3Dq is selectively expressed in noradrenergic neurons of the LC complex[16] (LC^{hM3Dq}) **(Fig. 2a)**. To test whether our chemogenetic strategy activates LC-NE neurons *in vivo*, we performed fiber photometry recordings in LC^{hM3Dq} mice and LC^{GFP} littermate controls following administration of clozapine N-oxide (CNO) or vehicle. Recordings revealed a sustained increase in LC-NE activity following CNO treatment in LC^{hM3Dq} mice compared to controls **(Fig. 2b)**. To compare the magnitude of LC^{hM3Dq} activation to a well-known stimulator of LC activity[17-22] and behaviors associated with stress and threat[23-25], we next administered the inhibitory Gi-coupled alpha-2 adrenergic receptor antagonist yohimbine (3 mg/kg i.p.). As expected, the "pharmacological stressor" yohimbine increased LC-NE activity relative to vehicle control **(Fig. 2b)**, and this effect was comparable in magnitude to LC^{hM3Dq} activation. Importantly, no effect of CNO or vehicle was observed in LC^{GFP} controls **(Fig. 2b**), suggesting the dynamics observed were unrelated to mouse movement. Together, the findings establish that our chemogenetic approach is effective in stimulating LC-NE activity *in vivo*.

To test if activation of LC-NE neurons would suppress feeding in hungry mice, LC^{hM3Dq} mice and littermate controls were overnight fasted and then treated with CNO or vehicle before placement in a novel arena containing standard chow **(Fig. 2c)**. In CNO-treated LC^{hM3Dq} mice, we found activation of LC-NE neurons suppressed feeding **(Fig. 2c)**. Importantly, CNO had no effect on the behavior of littermate controls **(Fig. 2c)**. These findings suggest that, despite the influence of hunger, activation of LC-NE neurons suppresses feeding in fasted mice.

To identify precisely how LC activation influences energy balance, we simultaneously measured feeding and metabolism of LC^{hM3Dq} and littermate control mice given drinking water with CNO (30 or 100 µg/mL) or plain water on alternate days **(Fig. 2d)**. In CNO-treated LC^{hM3Dq} mice, activation of LC-NE neurons dose-dependently suppressed feeding by reducing the amount of meals consumed**,** without affecting meal size **(Fig. 2d)**. Circadian analysis revealed

suppression of feeding occurred during lights-off when LC^{hM3Dq} mice drank the most CNO **(Supplementary Fig. 4).** This suppression of feeding was not observed during lights-on **(Supplementary Fig. 4)**, indicating that LC-mediated suppression of feeding was specific and reversible. Using indirect calorimetry to measure energy expenditure and respiratory exchange rate, we observed LC-NE activation had no effect on these metabolic endpoints **(Fig. 2d)**. Together these changes resulted in weight loss in CNO-treated LC^{hM3Dq} mice **(Fig. 2d)**. CNO had no effect on measures of feeding or metabolism in littermate controls **(Fig. 2d** and **Supplementary Fig. 4)**. These findings collectively demonstrate that activation of LC-NE neurons suppresses feeding without altering metabolism. Given our finding that LC activation selectively altered energy intake, in subsequent experiments we focused our observations to measures of feeding.

Since it is well known that LC-NE neurons co-express several neuropeptides[26-29], we next tested whether LC-mediated suppression of feeding depends on NE signaling. To selectively disrupt NE synthesis in LC neurons, we crossed our dopamine β-hydroxylase (*Dbh)* conditional knockout mice with $En1^{cre}$ (LC^{Dbh} mutants; unpublished reagent, NWP and PJ) **(Fig. 2e).** To increase LC activity[17-19] **(Fig. 2b)** and NE release[20-22], we pretreated LC^{Dbh} mutants and littermate controls with yohimbine (3 mg/kg i.p.) or vehicle and measured food intake. We found that baseline food intake was similar between LC^{Dbh} mutants and controls treated with vehicle **(Fig. 2f).** Food intake was significantly reduced in controls treated with yohimbine, but in contrast, yohimbine had no effect on feeding in LC^{Dbh} mutants **(Fig. 2f).** Because lack of LC-NE is the only difference between the mutants and controls, these findings suggest that LC neurons require norepinephrine for the observed suppression of feeding evoked by yohimbine. Measures of body weight revealed similar weight gain in adult LC^{Dbh} mutants and controls **(Fig. 2e)**, consistent with the full *Dbh* mutant that show deficits in NE does not produce excessive weight gain[30,31].

Prior studies have shown that NE has a strong inhibitory effect when applied directly in the lateral hypothalamus area (LHA)[32-34]. To determine if this effect is mediated by the LC, we measured Fos immunoreactivity in LC^{hM3Dq} mice following treatment of CNO or vehicle. Activation of LC-NE neurons resulted in a significant reduction in Fos expression in the LHA **(Supplementary Fig. 5a)**. To determine if this response was specific to the LHA, we measured Fos expression in two additional feeding-related targets of the LC, the dorsal medial and ventromedial hypothalamic nuclei. We observed no change in Fos expression in either nucleus **(Supplementary Fig. 5b)**.

To directly test whether enhanced activity in the LC-LHA circuit suppresses feeding, we injected AAVs expressing cre-dependent channelrhodopsin-2 (ChR2)[35,36] or eYFP in the LC of *Dbh*^{cre} mice **(Fig. 3a)**. Consistent with prior observations[37-39], we observed LC derived axons in the LHA that were labeled by eYFP **(Fig. 3b-c)**. $ChR2^{LC\text{-}LHA}$ and eYFP mice were next fasted overnight and food intake was measured in the presence or absence of photostimulation (**Fig. 3d)**. Given that high-power (20-mW total power) and high-frequency (>5 Hz) photostimulation of LC-NE soma has been shown to elicit reversible behavioral arrest[10], we used a photostimulation protocol (10-Hz, 10-ms pulses, ~7-mW total power) that has been shown to elicit high tonic rates of LC firing without behavioral arrests[38]. We revealed that $ChR2^{LC\text{-}LHA}$ mice had suppressed feeding during photostimulation compared to eYFP controls (**Fig. 3e)**. Importantly, photostimulation had no significant effect in eYFP controls and none of the manipulations affected locomotor activity (**Fig. 3e-g)**. Using this photostimulation protocol, we never observed a mouse that was immobilized in the recorded video or non-responsive to the experimenter directly after testing, confirming behavioral arrests were not observed in the present study. Furthermore, photostimulation of ChR2-expressing LHA terminals did not induce antidromic activity of LC-NE neurons as measured by Fos **(Supplementary Fig. 6).**

To determine if a shorter duration of stimulation would suppress feeding, we next used an epoch-based design wherein photostimulation was presented in alternating epochs or

withheld for the entire experiment in fasted mice (**Fig. 3h)**. When photostimulation was withheld, we observed a similar amount of feeding between ChR2$^{LC\text{-}LHA}$ and eYFP groups, wherein food intake was gradually decreased across the experiment as mice transitioned from hunger to satiety **(Fig. 3i)**. Similar feeding was also observed between ChR2$^{LC\text{-}LHA}$ and eYFP during the initial photostimulation epoch **(Fig. 3i)**, indicating stimulation of the LC-LHA pathway has no effect when hunger levels are at peak following a fast. In contrast, ChR2$^{LC\text{-}LHA}$ mice had suppressed feeding during the subsequent photostimulation epoch when hunger dampened compared to controls **(Fig. 3i-j)**. Taken together, the findings demonstrate stimulation of the LC-LHA pathway has a suppressive effect on feeding that may be modulated by hunger levels.

Since direct activation of LC-NE neurons enhances aversion and anxiety-like behaviors[16,38,40], we next tested if activation of the LC-LHA pathway would also enhanced these emotion-related responses. We therefore measured anxiety-like behavior of ChR2$^{LC\text{-}LHA}$ and eYFP mice in the open field test (OFT) and elevated plus maze (EPM) during photostimulation **(Supplementary Fig. 7a-b)**. We observed ChR2$^{LC\text{-}LHA}$ mice spent significantly less time in the center of the OFT **(Supplementary Fig. 7c)** and tended to spend less time in the open arms of the EPM **(Supplementary Fig. 7e)**, demonstrating that stimulating the LC-LHA pathway is anxiogenic. To assess if stimulation of the LC-LHA pathway has a negative or positive valence, we employed a real-time place preference test (RTPT) that triggers photostimulation upon entry into a designated side of the arena. We found ChR2$^{LC\text{-}LHA}$ mice spent less time in the stimulation-paired side compared to eYFP controls **(Supplementary Fig. 7g)**, indicating an aversive behavioral response resulting from LC-LHA circuit activation. Assessment of locomotor activity revealed ChR2$^{LC\text{-}LHA}$ mice had reduced ambulation in the OFT, but no change in the EPM and RTPT compared to eYFP control **(Supplementary Fig. 7d, f, h)**, suggesting the LC-LHA circuit does not have an overall impact on locomotion. Together, the findings demonstrate that activation of the LC-LHA pathway suppresses feeding, potentially due to an enhancement of negative valence.

To test if inhibition of the LC-LHA circuit enhances feeding, we injected AAVs expressing cre-dependent halorhodopsin (eNpHR3.0-eYFP) or eYFP in the LC of *Dbh*^{cre} mice **(Supplementary Fig. 8a-b)**. We next measured food intake in free-feeding eNpHR$^{LC\text{-}LHA}$ mice and controls during optical illumination. We observed similar food intake between eNpHR$^{LC\text{-}LHA}$ mice and eYFP controls (**Supplementary Fig. 8c)**. These findings, together with our prior optogenetic results, suggest that activation of the LC-LHA pathway suppresses feeding, but inhibition of the pathway does not promote feeding.

DISCUSSION

Collectively, we have demonstrated that endogenous activity of LC-NE neurons is suppressed during feeding in a manner modulated by nutritional state. We also found that activation of LC-NE neurons resulted in suppression of feeding through release of norepinephrine. Our experiments demonstrate that endogenous activity of LC-NE neurons is dynamically modulated during the consummatory sequence, with initial activation during food approach followed by a suppression of LC activity during consumption. This native pattern of LC-NE activity during consumption is unlikely attributed to changes in sleep, learning, stress or anxiety as our experimental mice were habituated to all aspects of the assay and they were tested during the portion of the circadian cycle when they are the most active. Instead, the approach-related LC response we observed likely reflects an appetitive response to food, in agreement with prior electrophysiological studies that show burst firing of LC neurons is associated with Pavlovian appetitive behavior in monkeys (e.g., lipping)[41]. Given LC neurons are well-known to modulate arousal[6,7,42,43], the decrease in LC activity we observed during feeding might reflect a decrease in arousal and/or disengagement with external sensory inputs to facilitate consummatory behavior.

Interestingly, we uncovered that suppression of LC-NE activity during consumption was gradually attenuated as mice approached satiety, indicating a previously unrecognized influence

of nutritional status on endogenous LC responses. Attenuation of the consummatory-related LC response could serve to direct attentional arousal from internal-to-external environment when energy levels transition from hunger to satiety, although additional research is needed to test this possibility. We also observed a loss of the approach-related LC response as hunger levels diminished, which may contribute to the decrease in salience of food as energy balance is restored. Such potential interpretation is congruent with integrative theories of LC-NE neurons which describe that this modulatory system is designed to optimize behavioral performance to a changing environment (as reviewed in [6,7,9]). These nutritional-state-related changes in LC-NE activity during feeding are not likely involved in coordinating some motor response, as locomotor activity remained stable across the trial, even as mice approached satiety (Supplementary Fig. 3).

While there have been hints that LC-NE neurons could be involved in the suppression of feeding[2,12,30,44-46], this possibility had not been directly tested. Experimentally determining a causal role for the LC-NE activity in feeding remained elusive using traditional lesion and genetic approaches. Physical lesions of the LC area had not produced a consistent change in feeding behavior[46-49], probably due to unreliable and nonselective effects. Further, although genetic ablation of dopamine beta-hydroxylase (*Dbh*) in mice had been linked to an elevation in food intake during cold stress[30], the contribution of the LC had remained unclear as the full *Dbh* knockout impacts all noradrenergic/adrenergic neurons in both the central and peripheral nervous systems. In the present study, we used chemogenetics to reveal a causal role for LC-NE activity in the suppression of feeding. Further, using our LC^{Dbh} mutants, we found that loss of LC-NE prevents the suppression of feeding evoked by yohimbine, which activated LC neurons **(Fig. 2b)**. Optogenetic stimulation of the LC→LHA pathway suppressed feeding while also enhancing aversion and anxiety-like behavior. In contrast, optogenetic inhibition of the LC-LHA pathway did not lead to an enhancement of feeding in freely feeding mice tested in a familiar cage. Together, our findings suggest that enhanced activity in LC-NE neurons suppresses

feeding but inhibition does not promote feeding. In context of the boarder LC literature, our findings suggest that LC-NE neurons are involved in the modulation of feeding by integrating both external cues (e.g., anxiogenic environmental cues) and internal drives (e.g., nutritional state).

Over four decades ago, a series of seminal studies established that direct delivery of NE agonists into the LHA suppressed feeding[50-54]. Using optogenetics, we have now revealed two previously unrecognized roles for a LC to LHA circuit: (1) the suppression of feeding and (2) enhancement of negative valence behavior (i.e., anxiety, aversion). This dual function is coherent with the well-established literature that shows LHA cell-types drive a variety of complex behaviors, including feeding, anxiety, and arousal[55-59]. An important future direction will be to determine whether the feeding and anxiety-related changes following LC-LHA pathway stimulation are mediated by separate or overlapping processes (e.g., target cell-types, receptor signaling mechanisms). Many cell-types may be involved, as prior electrophysiological studies have shown that NE has an inhibitory effect on the majority of LHA neurons[32-34,60,61].

Given the widespread projections of LC-NE neurons throughout the brain[37], it is likely that projections beyond hypothalamus are also involved in LC-NE modulation of feeding. It will be important to test this possibility using newly available tools to map, monitor and manipulate specific LC noradrenergic circuits. In sum, our findings expand upon established theories of LC function, which classically focus on arousal, emotion, memory and sleep[6,7,42,43,62], to include the modulation of feeding.

METHODS

Methods and associated references are available in the ***Supplemental information***.

SUPPLEMENTAL INFORMATION

Supplemental information can be found with this article.

ACKNOWLEDGEMENTS

We thank Madeline Hsaing, Kushal Prasad, and Janiece Morgan for technical assistance in behavioral and photometry experiments, as well as Juhee Haam for technical assistance with the photometry setup. We thank Social & Scientific Systems (Sandra McBride, Matthew Bridge, and Mike Easterling) for the custom code used to analyze photometry data (contract HHSN273201600011C with NIEHS). Valuable support was provided by the NIEHS Neurobehavioral, Fluorescence Microscopy and Imaging, and Viral Vector Cores. We thank the NIMH Drug Supply Program for providing the CNO. This research was supported by the Intramural Research Program of the NIH, NIEHS (ES102805 to PJ, ES103310 to GC) and NIDDK (DK075087 and DK075089 to MJK), and the Extramural Research Program of NIH (NIMH MH112355 to MRB).

AUTHOR CONTRIBUTIONS

NRS and PJ conceived, designed and supervised the project. Photometry experiments were performed by NRS and CMM under the guidance of GC and supervision of JDC. Feeding and metabolic experiments were performed by NRS, and analyzed by CAM, JA, JMP and NRS under the guidance of AVK and MJK. Optogenetic experiments were performed by NRS under the guidance of MRB, MJK, and JDC. NP created the *Dbh*^{cre} and *Dbh*^{cKO} alleles and Flp-dependent viral vectors. IE characterized the *Dbh*^{cKO} allele. Immunohistochemistry, *in situ* hybridization, and image acquisition was performed by NRS, KGS, JA, CYK and JP. Cell counts were performed by SAF and CXY. NRS and PJ wrote the manuscript with input from coauthors.

DECLARATION OF INTERESTS

The authors declare no competing financial interests.

REFERENCES

1 Hobson, J. A., McCarley, R. W. & Wyzinski, P. W. Sleep cycle oscillation: reciprocal discharge by two brainstem neuronal groups. *Science* **189**, 55-58, doi:10.1126/science.1094539 (1975).

2 Aston-Jones, G. & Bloom, F. E. Norepinephrine-containing locus coeruleus neurons in behaving rats exhibit pronounced responses to non-noxious environmental stimuli. *J Neurosci* **1**, 887-900 (1981).

3 Rasmussen, K., Morilak, D. A. & Jacobs, B. L. Single unit activity of locus coeruleus neurons in the freely moving cat. I. During naturalistic behaviors and in response to simple and complex stimuli. *Brain Res* **371**, 324-334 (1986).

4 Grant, S. J., Aston-Jones, G. & Redmond, D. E., Jr. Responses of primate locus coeruleus neurons to simple and complex sensory stimuli. *Brain Res Bull* **21**, 401-410 (1988).

5 Herve-Minvielle, A. & Sara, S. J. Rapid habituation of auditory responses of locus coeruleus cells in anaesthetized and awake rats. *Neuroreport* **6**, 1363-1368 (1995).

6 Sara, S. J. & Bouret, S. Orienting and reorienting: the locus coeruleus mediates cognition through arousal. *Neuron* **76**, 130-141, doi:10.1016/j.neuron.2012.09.011 (2012).

7 Aston-Jones, G. & Cohen, J. D. An integrative theory of locus coeruleus-norepinephrine function: adaptive gain and optimal performance. *Annu Rev Neurosci* **28**, 403-450, doi:10.1146/annurev.neuro.28.061604.135709 (2005).

8 Berridge, C. W., Schmeichel, B. E. & Espana, R. A. Noradrenergic modulation of wakefulness/arousal. *Sleep Med Rev* **16**, 187-197, doi:10.1016/j.smrv.2011.12.003 (2012).

9 Aston-Jones, G. & Waterhouse, B. Locus coeruleus: From global projection system to adaptive regulation of behavior. *Brain Res* **1645**, 75-78, doi:10.1016/j.brainres.2016.03.001 (2016).

10 Carter, M. E. *et al.* Tuning arousal with optogenetic modulation of locus coeruleus neurons. *Nat Neurosci* **13**, 1526-1533, doi:10.1038/nn.2682 (2010).

11 Vazey, E. M. & Aston-Jones, G. Designer receptor manipulations reveal a role of the locus coeruleus noradrenergic system in isoflurane general anesthesia. *Proc Natl Acad Sci U S A* **111**, 3859-3864, doi:10.1073/pnas.1310025111 (2014).

12 Grant, S. J. & Redmond, D. E., Jr. Neuronal activity of the locus ceruleus in awake Macaca arctoides. *Exp Neurol* **84**, 701-708 (1984).

13 Meng, C. *et al.* Spectrally Resolved Fiber Photometry for Multi-component Analysis of Brain Circuits. *Neuron* **98**, 707-717 e704, doi:10.1016/j.neuron.2018.04.012 (2018).

14 Foote, S. L., Aston-Jones, G. & Bloom, F. E. Impulse activity of locus coeruleus neurons in awake rats and monkeys is a function of sensory stimulation and arousal. *Proc Natl Acad Sci U S A* **77**, 3033-3037 (1980).

15 Nguyen, K. P., O'Neal, T. J., Bolonduro, O. A., White, E. & Kravitz, A. V. Feeding Experimentation Device (FED): A flexible open-source device for measuring feeding behavior. *J Neurosci Methods* **267**, 108-114, doi:10.1016/j.jneumeth.2016.04.003 (2016).

16 Sciolino, N. R. *et al.* Recombinase-Dependent Mouse Lines for Chemogenetic Activation of Genetically Defined Cell Types. *Cell Rep* **15**, 2563-2573, doi:10.1016/j.celrep.2016.05.034 (2016).

17 Goldstein, J. M., Knobloch, L. C. & Malick, J. B. Electrophysiological demonstration of both alpha 2-agonist and antagonist properties of RX 781094. *Eur J Pharmacol* **91**, 101-105, doi:10.1016/0014-2999(83)90368-0 (1983).

18 Pitts, D. K. & Marwah, J. Electrophysiological actions of cocaine on noradrenergic neurons in rat locus ceruleus. *J Pharmacol Exp Ther* **240**, 345-351 (1987).

19 Osaka, T. & Matsumura, H. Noradrenergic inputs to sleep-related neurons in the preoptic area from the locus coeruleus and the ventrolateral medulla in the rat. *Neurosci Res* **19**, 39-50 (1994).

20 Abercrombie, E. D., Keller, R. W., Jr. & Zigmond, M. J. Characterization of hippocampal norepinephrine release as measured by microdialysis perfusion: pharmacological and behavioral studies. *Neuroscience* **27**, 897-904 (1988).

21 Duggan, S., Hong, M., Milne, B. & Jhamandas, K. The role of excitatory amino acids in the expression of precipitated acute and chronic clonidine withdrawal: an in vivo voltammetric study in the rat locus coeruleus. *Brain Res* **665**, 253-261, doi:10.1016/0006-8993(94)91345-5 (1994).

22 Park, J., Kile, B. M. & Wightman, R. M. In vivo voltammetric monitoring of norepinephrine release in the rat ventral bed nucleus of the stria terminalis and anteroventral thalamic nucleus. *Eur J Neurosci* **30**, 2121-2133, doi:10.1111/j.1460-9568.2009.07005.x (2009).

23 Holmes, A., Yang, R. J. & Crawley, J. N. Evaluation of an anxiety-related phenotype in galanin overexpressing transgenic mice. *J Mol Neurosci* **18**, 151-165, doi:10.1385/JMN:18:1-2:151 (2002).

24 Bhattacharya, S. K., Mitra, S. K. & Acharya, S. B. Anxiogenic activity of isatin, a putative biological factor, in rodents. *J Psychopharmacol* **5**, 202-206, doi:10.1177/026988119100500304 (1991).

25 Thiebot, M. H., Soubrie, P., Doare, L. & Simon, P. Evidence against the involvement of a noradrenergic mechanism in the release by diazepam of novelty-induced hypophagia in rats. *Eur J Pharmacol* **100**, 201-205 (1984).

26 Charnay, Y. *et al.* Evidence for the presence of enkephalin in catecholaminergic neurones of cat locus coeruleus. *Neurosci Lett* **30**, 147-151 (1982).

27 Sofroniew, M. V. Vasopressin- and neurophysin-immunoreactive neurons in the septal region, medial amygdala and locus coeruleus in colchicine-treated rats. *Neuroscience* **15**, 347-358 (1985).

28 Cortes, R., Ceccatelli, S., Schalling, M. & Hokfelt, T. Differential effects of intracerebroventricular colchicine administration on the expression of mRNAs for neuropeptides and neurotransmitter enzymes, with special emphasis on galanin: an in situ hybridization study. *Synapse* **6**, 369-391, doi:10.1002/syn.890060410 (1990).

29 Nishio, T. *et al.* Cellular localization of nerve growth factor-like immunoreactivity in adult rat brain: quantitative and immunohistochemical study. *Neuroscience* **60**, 67-84 (1994).

30 Thomas, S. A. & Palmiter, R. D. Thermoregulatory and metabolic phenotypes of mice lacking noradrenaline and adrenaline. *Nature* **387**, 94-97, doi:10.1038/387094a0 (1997).

31 Ste Marie, L., Luquet, S., Curtis, W. & Palmiter, R. D. Norepinephrine- and epinephrine-deficient mice gain weight normally on a high-fat diet. *Obes Res* **13**, 1518-1522, doi:10.1038/oby.2005.185 (2005).

32 Karadi, Z. *et al.* Responses of lateral hypothalamic glucose-sensitive and glucose-insensitive neurons to chemical stimuli in behaving rhesus monkeys. *J Neurophysiol* **67**, 389-400 (1992).

33 Nishino, H., Oomura, Y., Aou, S. & Lenard, L. Catecholaminergic mechanisms of feeding-related lateral hypothalamic activity in the monkey. *Brain Res* **405**, 56-67 (1987).

34 Li, Y. & van den Pol, A. N. Direct and indirect inhibition by catecholamines of hypocretin/orexin neurons. *J Neurosci* **25**, 173-183, doi:10.1523/JNEUROSCI.4015-04.2005 (2005).

35 Atasoy, D., Aponte, Y., Su, H. H. & Sternson, S. M. A FLEX switch targets Channelrhodopsin-2 to multiple cell types for imaging and long-range circuit mapping. *J Neurosci* **28**, 7025-7030, doi:10.1523/JNEUROSCI.1954-08.2008 (2008).

36 Schnutgen, F. *et al.* A directional strategy for monitoring Cre-mediated recombination at the cellular level in the mouse. *Nat Biotechnol* **21**, 562-565, doi:10.1038/nbt811 (2003).

37 Robertson, S. D., Plummer, N. W., de Marchena, J. & Jensen, P. Developmental origins of central norepinephrine neuron diversity. *Nat Neurosci* **16**, 1016-1023, doi:10.1038/nn.3458 (2013).

38 McCall, J. G. *et al.* CRH Engagement of the Locus Coeruleus Noradrenergic System Mediates Stress-Induced Anxiety. *Neuron* **87**, 605-620, doi:10.1016/j.neuron.2015.07.002 (2015).

39 Palkovits, M. *et al.* Noradrenergic innervation of the rat hypothalamus:experimental biochemical and electron microscopic studies. *Brain Res* **191**, 161-171 (1980).

40 McCall, J. G. *et al.* Locus coeruleus to basolateral amygdala noradrenergic projections promote anxiety-like behavior. *Elife* **6**, doi:10.7554/eLife.18247 (2017).

41 Bouret, S. & Richmond, B. J. Sensitivity of locus ceruleus neurons to reward value for goal-directed actions. *J Neurosci* **35**, 4005-4014, doi:10.1523/JNEUROSCI.4553-14.2015 (2015).

42 Berridge, C. W. & Waterhouse, B. D. The locus coeruleus-noradrenergic system: modulation of behavioral state and state-dependent cognitive processes. *Brain Res Brain Res Rev* **42**, 33-84 (2003).

43 Bouret, S. & Sara, S. J. Network reset: a simplified overarching theory of locus coeruleus noradrenaline function. *Trends Neurosci* **28**, 574-582, doi:10.1016/j.tins.2005.09.002 (2005).

44 Tovar, S. *et al.* K(ATP)-channel-dependent regulation of catecholaminergic neurons controls BAT sympathetic nerve activity and energy homeostasis. *Cell Metab* **18**, 445-455, doi:10.1016/j.cmet.2013.08.006 (2013).

45 Bello, N. T., Yeh, C. Y., Verpeut, J. L. & Walters, A. L. Binge-like eating attenuates nisoxetine feeding suppression, stress activation, and brain norepinephrine activity. *PLoS One* **9**, e93610, doi:10.1371/journal.pone.0093610 (2014).

46 Redmond, D. E., Jr., Huang, Y. H., Snyder, D. R., Maas, J. W. & Baulu, J. Hyperphagia and hyperdipsia after locus coeruleus lesions in the stumptailed monkey. *Life Sci* **20**, 1619-1628 (1977).

47 Ahlskog, J. E. & Hoebel, B. G. Overeating and obesity from damage to a noradrenergic system in the brain. *Science* **182**, 166-169 (1973).

48 Anlezark, G. M., Crow, T. J. & Greenway, A. P. Impaired learning and decreased cortical norepinephrine after bilateral locus coeruleus lesions. *Science* **181**, 682-684 (1973).

49 Kubiak, P. & Zagrodzka, J. DSP-4 lesion of locus coeruleus does not affect spontaneous predatory behaviour in cats. *Acta Neurobiol Exp (Wars)* **53**, 525-534 (1993).

50 Leibowitz, S. F. Reciprocal hunger-regulating circuits involving alpha- and beta-adrenergic receptors located, respectively, in the ventromedial and lateral hypothalamus. *Proc Natl Acad Sci U S A* **67**, 1063-1070 (1970).

51 Margules, D. L., Lewis, M. J., Dragovich, J. A. & Margules, A. S. Hypothalamic norepinephrine: circadian rhythms and the control of feeding behavior. *Science* **178**, 640-643 (1972).

52 Margules, D. L. Alpha-adrenergic receptors in hypothalamus for the suppression of feeding behavior by satiety. *J Comp Physiol Psychol* **73**, 1-12 (1970).

53 Capuano, C. A., Leibowitz, S. F. & Barr, G. A. The pharmaco-ontogeny of the perifornical lateral hypothalamic beta 2-adrenergic and dopaminergic receptor systems mediating epinephrine- and dopamine-induced suppression of feeding in the rat. *Brain Res Dev Brain Res* **70**, 1-7 (1992).

54 Booth, D. A. Localization of the adrenergic feeding system in the rat diencephalon. *Science* **158**, 515-517 (1967).

55 Brown, J. A., Woodworth, H. L. & Leinninger, G. M. To ingest or rest? Specialized roles of lateral hypothalamic area neurons in coordinating energy balance. *Front Syst Neurosci* **9**, 9, doi:10.3389/fnsys.2015.00009 (2015).

56 Stuber, G. D. & Wise, R. A. Lateral hypothalamic circuits for feeding and reward. *Nat Neurosci* **19**, 198-205, doi:10.1038/nn.4220 (2016).

57 Bonnavion, P., Mickelsen, L. E., Fujita, A., de Lecea, L. & Jackson, A. C. Hubs and spokes of the lateral hypothalamus: cell types, circuits and behaviour. *J Physiol* **594**, 6443-6462, doi:10.1113/JP271946 (2016).

58 Qualls-Creekmore, E. & Munzberg, H. Modulation of Feeding and Associated Behaviors by Lateral Hypothalamic Circuits. *Endocrinology*, doi:10.1210/en.2018-00449 (2018).

59 Cassidy, R. M. *et al.* A lateral hypothalamus to basal forebrain neurocircuit promotes feeding by suppressing responses to anxiogenic environmental cues. *Sci Adv* **5**, eaav1640, doi:10.1126/sciadv.aav1640 (2019).

60 Grivel, J. *et al.* The wake-promoting hypocretin/orexin neurons change their response to noradrenaline after sleep deprivation. *J Neurosci* **25**, 4127-4130, doi:10.1523/JNEUROSCI.0666-05.2005 (2005).

61 Gao, X. B., Ghosh, P. K. & van den Pol, A. N. Neurons synthesizing melanin-concentrating hormone identified by selective reporter gene expression after transfection in vitro: transmitter responses. *J Neurophysiol* **90**, 3978-3985, doi:10.1152/jn.00593.2003 (2003).

62 Arnsten, A. F. & Li, B. M. Neurobiology of executive functions: catecholamine influences on prefrontal cortical functions. *Biol Psychiatry* **57**, 1377-1384, doi:10.1016/j.biopsych.2004.08.019 (2005).

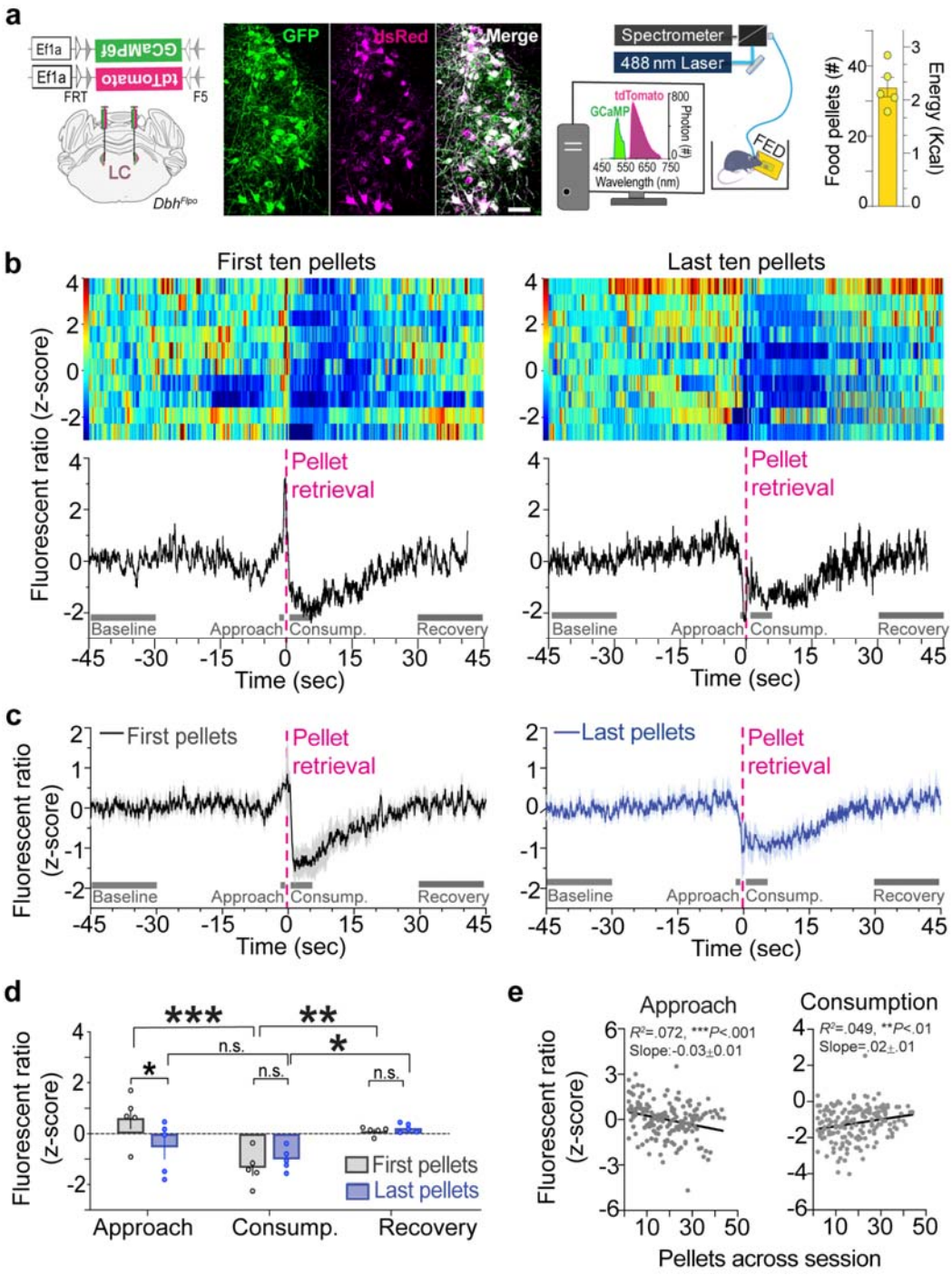

Figure 1. Activity of LC-NE neurons is increased during food approach and suppressed during feeding in a manner influenced by nutritional state. (a) *Top.* Flp-dependent viral genetic strategy for co-expression of GCaMP6f and tdTomato in LC-NE neurons. *Middle.* Coronal view of the locus coeruleus from a $LC^{GCaMP/tdT}$ mouse immunostained for GCaMP6f

(GFP antibody) and tdTomato (dsRed antibody). Schematic of *in vivo* fiber photometry setup and feeding experimentation device (FED). *Right.* Average energy intake across the 1-hr session. Data are mean ± SEM. n=5 fasted $LC^{GCaMP/tdT}$ mice. **(b)** Example response around pellet retrieval of a fasted mouse expressing a fluorescent ratio of GCaMP6f/tdTomato in LC neurons during the first ten pellets (*left*) and last ten pellets of the session (*right*). Single trials are represented in the heat map, whereas the average z-score fluorescent ratio is represented in the trace below. **(c)** Average z-score fluorescent ratio aligned-to-pellet retrieval in fasted mice during the first ten pellets (*left*) and last ten pellets of the session (*right*). Data are mean ± SEM. n=5 $LC^{GCaMP/tdT}$ mice. **(d)** Average z-score fluorescent ratio during feeding-related behaviors. Two-way repeated measures ANOVA, nutritional state x behavior interaction: $F_{2,\ 8}$= 7.018, P=0.0174. Bonferroni post-hoc test ***P<0.001, **P<0.01, and *P<0.05. Data are mean ± SEM. n=5 $LC^{GCaMP/tdT}$ mice. **(e)** Linear regression of the average fluorescent ratio during food approach and consumption in relation to pellet events across the session in $LC^{GCaMP/tdT}$ mice following an overnight fast. Approach (R^2=0.072; $F_{1,168}$=13.06, P<0.001) and Consumption (R^2=0.049; $F_{1,168}$=8.05, **P<0.01).

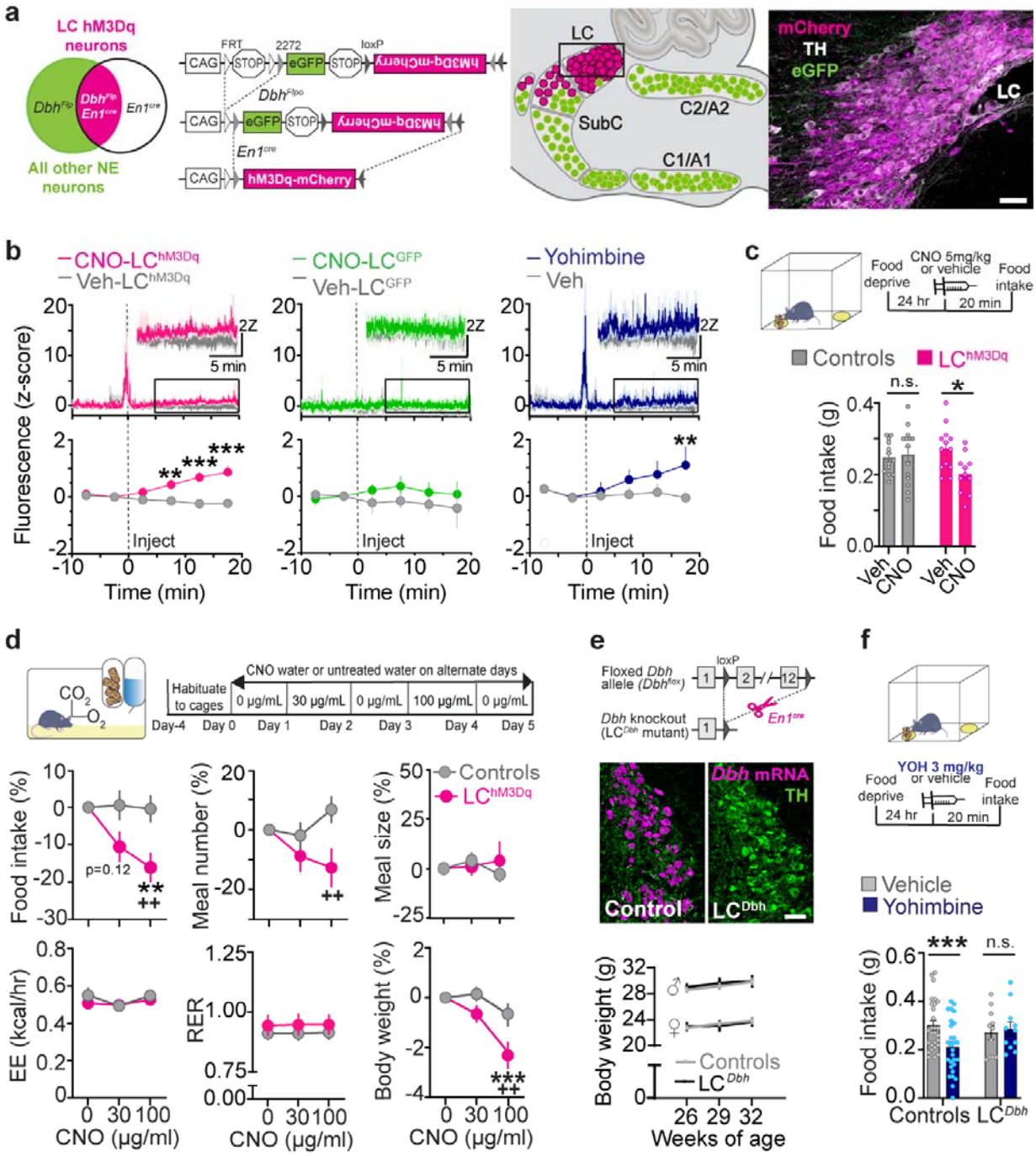

Figure 2. Activation of LC-NE neurons suppresses feeding in a manner dependent on norepinephrine signaling. (a) *Left.* Schematic illustration of intersectional genetic strategy. Recombination of *RC::FL-hM3Dq* allele by *Dbh*^{Flpo} and *En1*^{cre} results in LC-selective hM3Dq-mCherry expression. Recombination by *Dbh*^{Flpo} alone leads to eGFP expression. *Right.* Schematic shows a mouse hindbrain compressed across the sagittal axis. Parasagittal section

from LC^{hM3Dq} brain reveals hM3Dq-mCherry expression in LC-NE neurons. Scale, 50 μm. **(b)** *Top.* Average z-score fluorescence aligned to injection time in LC^{hM3Dq} mice expressing either GCaMP6f or GCaMP6f/tdTomato treated with clozapine n-oxide (CNO; magenta), yohimbine (blue) or vehicle (gray), and in LC^{GFP} mice treated with CNO (green) or vehicle (gray). In all mice, except LC^{GFP} controls, we detected a transient increase in LC-NE activity in response to an experimenter approaching for injection, demonstrating the sensitivity of our recording conditions to detect an established visual threat response characterized previously[3,4,14]. *Bottom.* Quantification of average z-score fluorescence following CNO (5 mg/kg i.p.) or yohimbine (3 mg/kg i.p.) treatment. Two-way repeated measures ANOVA, drug x time interaction: LC^{hM3Dq} ($F_{5, 35}$= 9.157, P=0.0001), LC^{GFP} ($F_{5, 20}$= 0.4994, P=0.7730), LC-Yohimbine ($F_{5, 20}$= 2.592, P=0.0579). Bonferroni post-hoc, ***P<0.01, **P<0.01 vs. vehicle, n=8 LC^{hM3Dq} mice. n=5 LC^{GFP} mice. n=5 mice for yohimbine-LC experiment. Data are mean ± SEM. **(c)** *Top.* Timeline of acute food intake experiments in fasted mice. *Bottom.* Average food intake in fasted mice. Two-way between subject's ANOVA, drug x genotype interaction: $F_{1, 47}$= 5.2, P=0.0272. Bonferroni posthoc test, *P<0.05. n=13 vehicle-treated and n=14 CNO-treated littermate controls. n=13 vehicle-treated and n=11 CNO-treated LC^{hM3Dq} mice. **(d)** *Top.* Timeline of CNO water dosing at 30 and 100 μg/mL. Note that this method delivered a daily total dose of approximately 4 or 10 mg/kg CNO. *Bottom.* Measures in the automated homecage test. Two-way repeated measures ANOVA, drug x genotype interaction: food intake ($F_{2, 54}$= 3.59, P=0.0343), meal number ($F_{2, 54}$= 3.44, P=0.0393), meal size ($F_{2,54}$= 0.864, P=0.4271), energy expenditure (EE, $F_{2, 54}$= 0.22, P=0.8036), respiratory exchange rate (RER, $F_{2,54}$= 0.0509, P=0.9504), and body weight ($F_{2, 70}$= 3.65, P=0.031). Bonferroni posthoc test, ***P<0.001, **P<0.01 vs. vehicle; $^{++}$P<0.01 vs. littermate controls. n=20 littermate controls. n=9 LC^{hM3Dq} mice for all measures (expect body weight wherein n=17 LC^{hM3Dq} mice). Data are mean ± SEM. **(e)** *Top.* Schematic diagram of *Dbh cKO* allele. Recombination by $En1^{cre}$ leads to disruption of norepinephrine synthesis in LC-NE neurons. *Middle*. Coronal brain sections stained for *Dbh* (riboprobe; magenta) and tyrosine

hydroxylase (TH antibody; green). Scale, 50-μm. *Bottom.* Two-way repeated subject's ANOVA, time x genotype interaction: $F_{6,114}$= 0.77, P=0.5925. n=18-19 littermate controls, n=11-13 LC^{Dbh} mutants. Data are ± SEM. **(f)** Food intake in fasted mice treated with yohimbine (3 mg/kg, i.p.). Two-way repeated measures ANOVA, drug x genotype interaction: $F_{1,37}$= 10.8, P<0.0022. Bonferroni posthoc test, ***P<0.001 vs vehicle. n.s., non-significant. n=28 littermate controls, n=11 LC^{Dbh} mutants. Data are ± SEM.

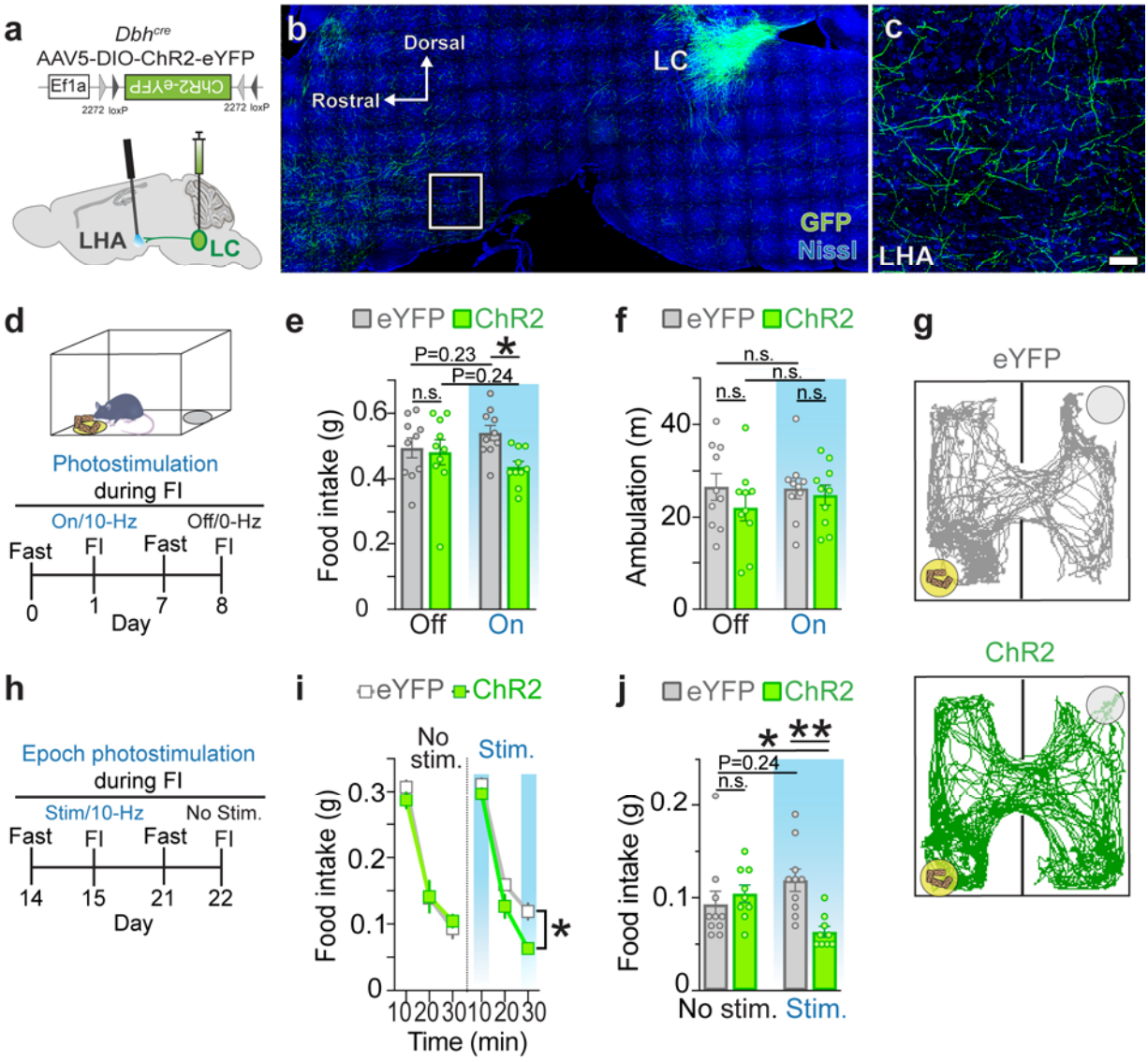

Figure 3. Stimulation of LC-LHA noradrenergic circuit suppresses feeding. (a) Schematic illustration of sagittal mouse brain shows location of cre-dependent AAV used to drive ChR2-eYFP expression and location of fiberoptic probes. **(b-c)** Parasagittal brain section from a *Dbh*^{cre}; eYFP$^{LC\rightarrow LHA}$ mouse shows restricted eYFP expression in LC-NE neurons. High magnification image shows eYFP-expressing LC-NE axonal projections in the LHA. Scale is 400-μm (brain) and 150-μm (LHA). **(d)** Timeline of photostimulation (10-Hz, 10-ms pulses) during food intake (FI) test. **(e-f)** Feeding-related behaviors in fasted mice. Two-way repeated measure ANOVA, Stimulation x Virus interaction: food intake (**e**, $F_{1,\ 18}$= 5.44, P=0.0314) and

ambulation (**f**, $F_{1, 18}$= 0.655, *P*=0.4290), Bonferroni posthoc test, **P*<0.05. *n*=10 eYFP$^{LC\text{-}LHA}$ mice, n=10 ChR2$^{LC\text{-}LHA}$ mice. Data are mean ± SEM. **(g)** Representative traces shows ambulation in the feeding task during photostimulation. Yellow circle indicates the location of the food cup and gray circle indicates location of the empty cup. **(h)** Timeline of epoch photostimulation (10-Hz, 10-ms pulses) during food intake. **(i-j)** Food intake in fasted mice during entire epoch experiment (i) and last epoch bin (j). Three-way repeated measure ANOVA, Stimulation x Virus x Time interaction: (**i**, $F_{2,34}$= 3.646, *P*=0.037) and Time main effect (**i**, $F_{2,34}$= 295.996, *P*<0.001). Two-way repeated measure ANOVA, Stimulation x Virus interaction (**j**, $F_{1,17}$= 8.57, *P*=0.0094). Bonferroni posthoc test, ***P*<0.01, **P*<0.05 ChR2 vs. eYFP during second photostimulation epoch. *n*=10 eYFP$^{LC\text{-}LHA}$ mice, n=9 ChR2$^{LC\text{-}LHA}$ mice. Data are mean ± SEM. n.s., non-significant.

SUPPLEMENTARY INFORMATION

Supplemental Figures

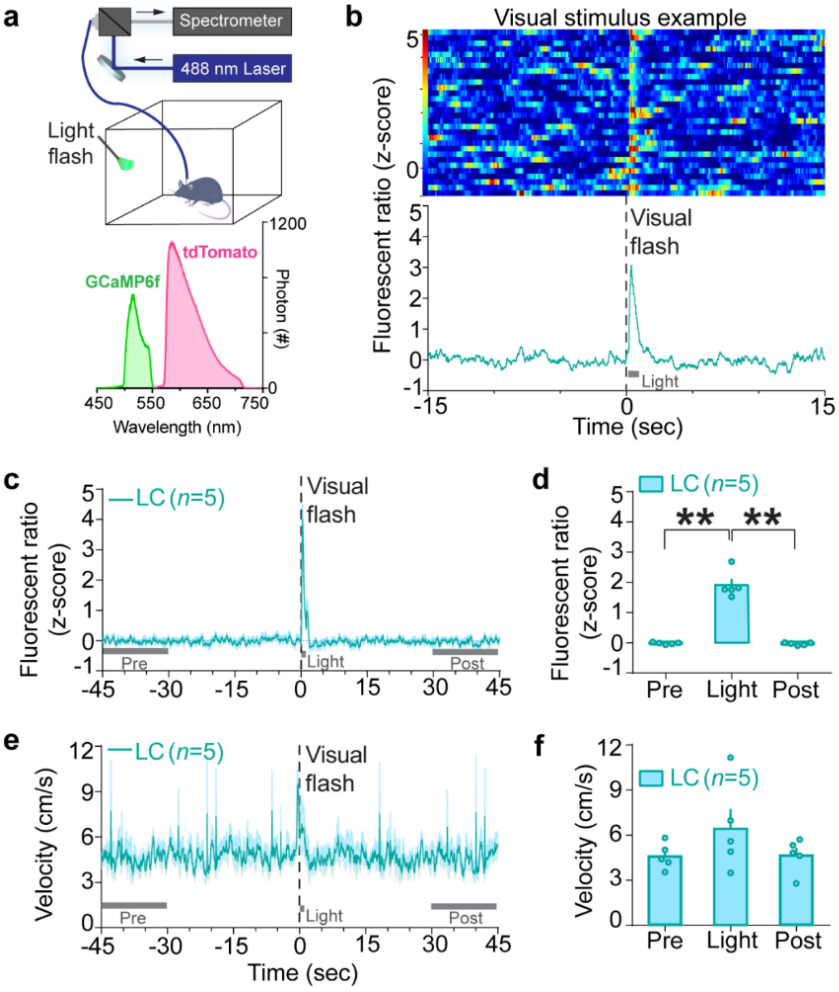

Supplementary Figure 1. LC calcium activity is increased by a visual stimulus. (a) *Top*. Schematic of *in vivo* fiber photometry setup and light source used to deliver the visual flash. *Bottom*. Representative fluorescent emission spectrum during photometry recordings. Data shown is an average signal of GCaMP6f and tdTomato emission spectra across 25 frames from a representative $LC^{GCaMP/tdT}$ mouse. **(b)** Example fluorescent ratio expressed as z-score aligned-to-visual stimulus in a $LC^{GCaMP/tdT}$ mouse. Single trials are represented in the heat map, whereas the average z-score fluorescent ratio is represented in the trace below. **(c-d)** Average z-score fluorescent ratio aligned-to-visual stimulus (c) and during visual-related events (d). One-way

repeated measures ANOVA ($F_{1,4}$=7.78, P<0.05). **P<0.01 (Bonferroni). Data are mean ± SEM. n=5 $LC^{GCaMP/tdT}$ mice mice. **(e-f)** Average velocity aligned-to-visual stimulus (e) and during visual-related events (f). One-way repeated measures ANOVA ($F_{1,4}$=3.101, P=0.15). Data are mean ± SEM. n=5 $LC^{GCaMP/tdT}$ mice.

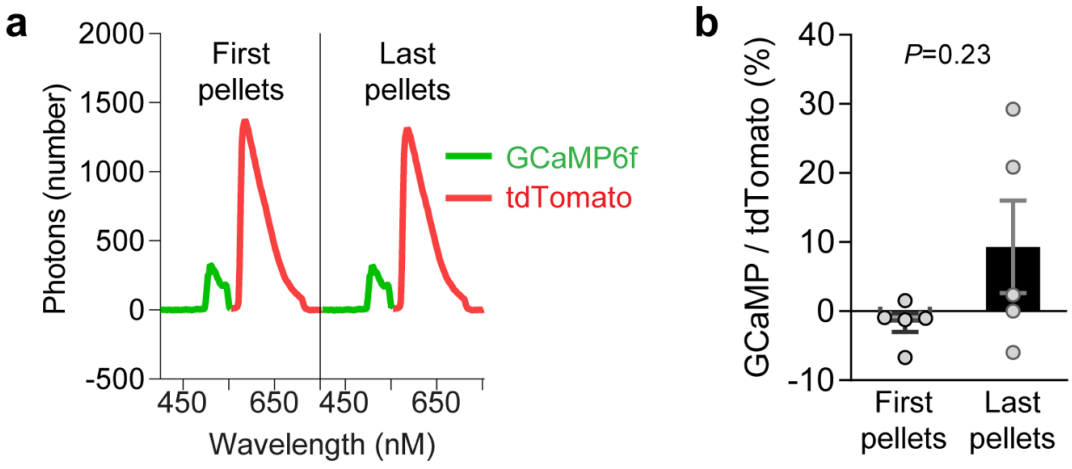

Supplementary Figure 2. No significant change in baseline activity of LC-NE neurons as mice consumed more across the trial. (a) Fluorescent emission spectrum from a representative $LC^{GCaMP/tdT}$ mouse across 15-sec baseline windows before the first and last ten pellets of the recording session. **(b)** Average ratio of GCaMP6f to tdTomato expressed as a percentage of the initial 15-sec baseline period in the session prior to consumption. Paired samples *t*-test (t_4=1.41, *P*=0.231). Data are mean ± SEM. *n*=5 $LC^{GCaMP/tdT}$ mice.

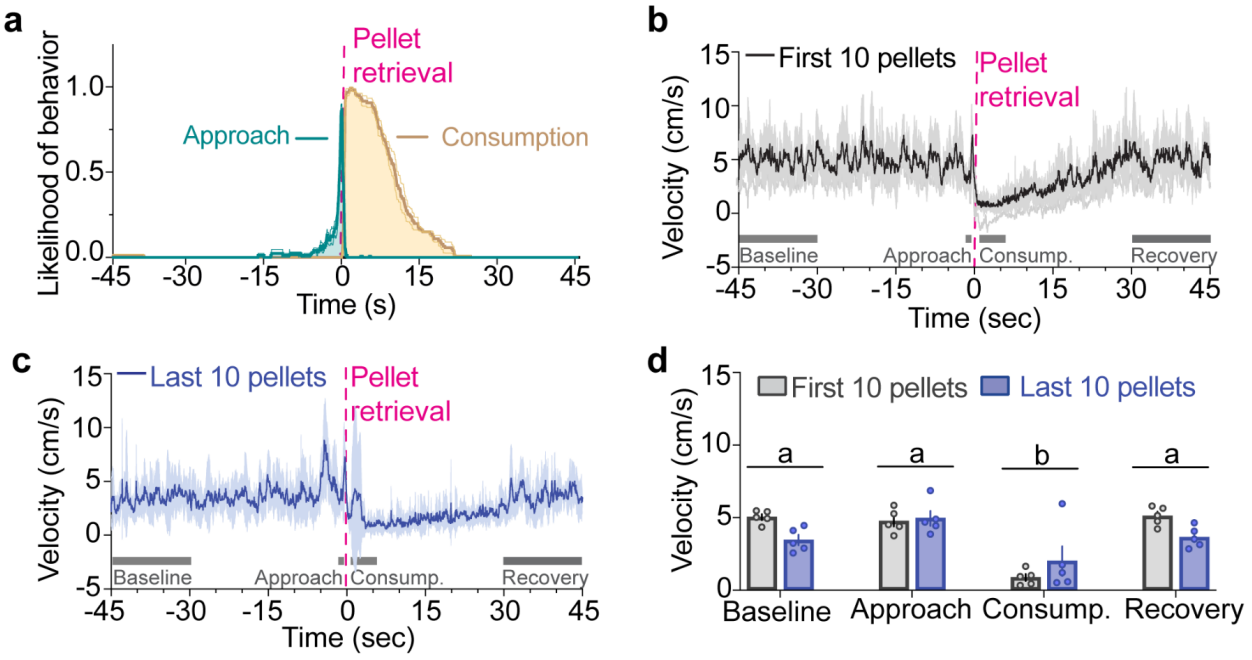

Supplementary Figure 3. Movement velocity is suppressed during feeding independent of nutritional state. (a) Likelihood of feeding-related behavior surrounding pellet retrieval in $LC^{GCaMP/tdT}$ mice following an overnight fast. Data are mean ± SEM. *n*=3 $LC^{GCaMP/tdT}$ mice. **(b-c)** Average velocity aligned-to-pellet retrieval in $LC^{GCaMP/tdT}$ mice during the first ten pellets (b) and last ten pellets of the session (c). Data are mean ± SEM. *n*=5 $LC^{GCaMP/tdT}$ mice. **(d)** Average velocity during feeding-related behaviors. Two-way repeated measures ANOVA. Main effect of behavior: $F_{3,12}$=22.14, P<0.001. Bonferroni post hoc test, P<0.01 consumption (group b) vs. all other behavioral states (group a). Data are mean ± SEM. *n*=5 $LC^{GCaMP/tdT}$ mice.

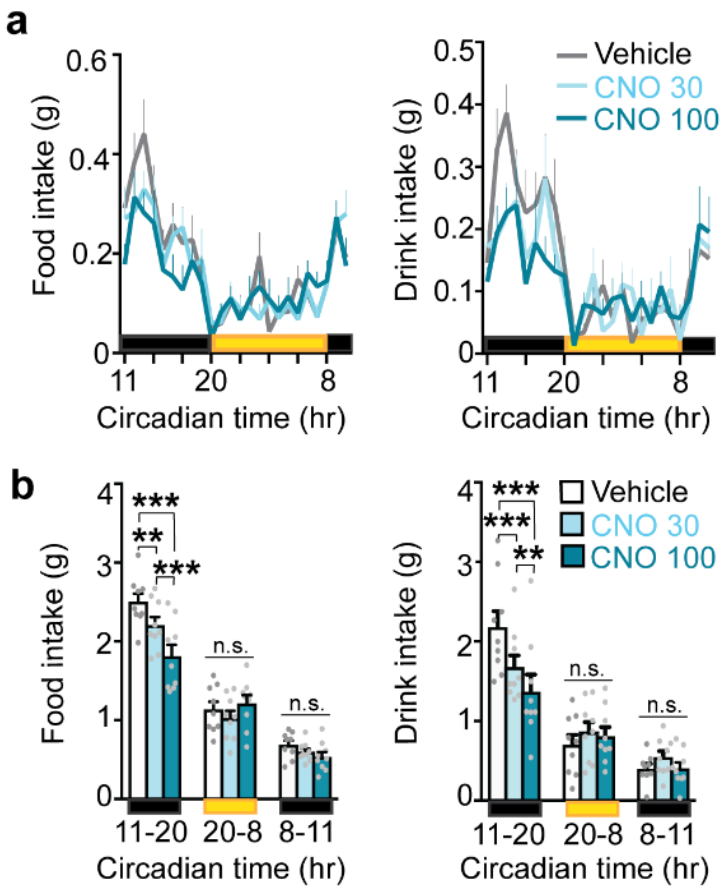

Supplementary Figure 4. Circadian analysis reveals chemogenetic activation of LC-NE neurons suppresses feeding and drinking in a specific- and reversible manner. (a). Circadian food and drink intake by LC^{hM3Dq} mice receiving CNO (30 and 100 μg/mL) in drinking water. **(b).** Average intake of food and drink during the 24-hour circadian light cycle. Repeated measures ANOVA drug x time interaction: food intake (**b**, $F_{4,32}$= 12.0, P<0.0001) and drink intake (**d**, $F_{4,32}$= 21.4, P<0.0001). Bonferroni posthoc test, ***P<0.001, **P<0.01. n=9 LC^{hM3Dq} mice. Data are ± SEM. CT, circadian time. Yellow shows circadian lights-on (CT 20-8). Black shows circadian lights-off, which was divided according to when drug was first introduced (CT 11-20; early dark) and later present (CT 8-11; late dark). n.s., non-significant.

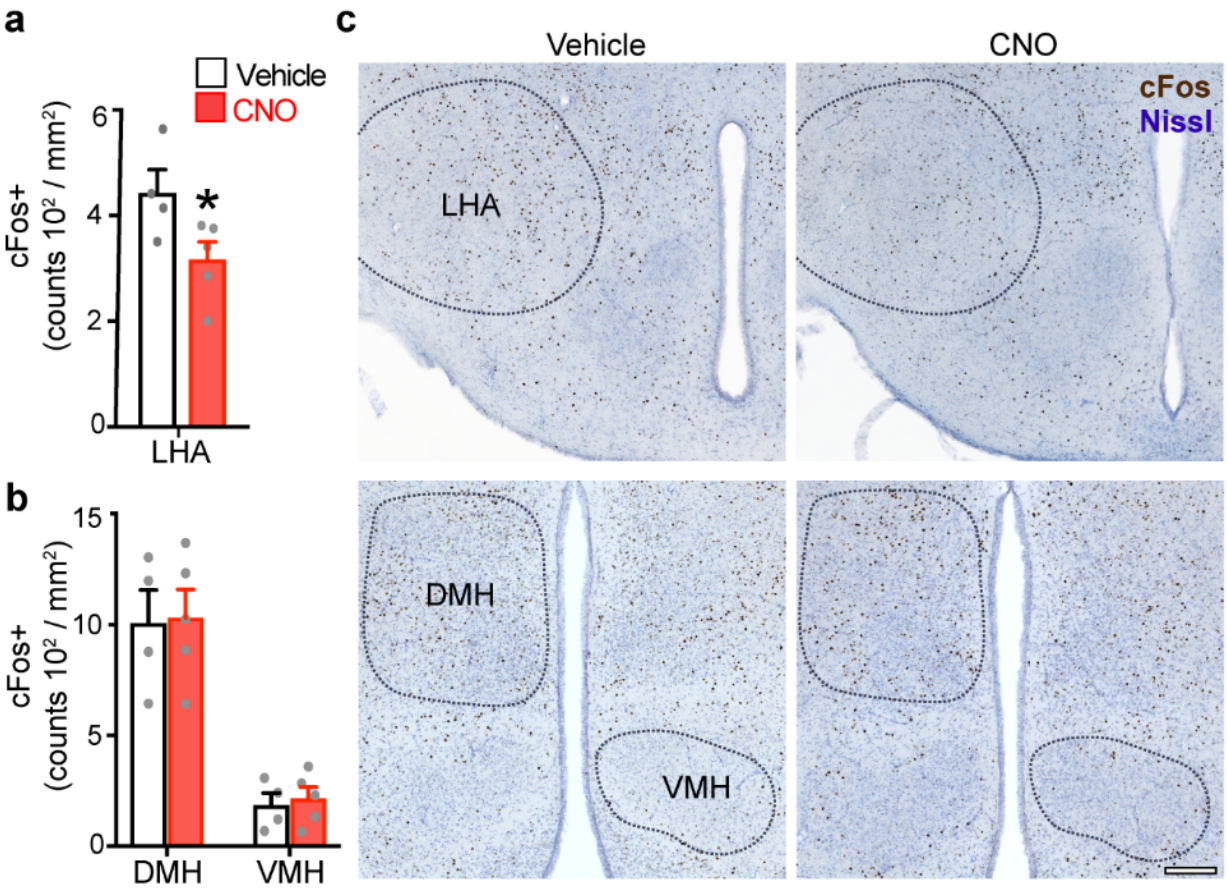

Supplementary Figure 5. Chemogenetic activation of LC-NE neurons selectively reduces neuronal activity in the LHA. **(a-b)** Average Fos+ cell counts in the LHA of LC^{hM3Dq} mice. Unpaired samples t-test (one-tailed): LHA (**a**, t_7=2.302, **P*=0.0274), DMH (**b**, t_7=0.1281, *P*=0.4509), and VMH (**b**, t_7=0.3852, *P*=0.3558). Data are mean ± SEM. n=4 vehicle mice, n=5 CNO (1-mg/kg i.p.) mice. **(c)** Immunofluorescent labeling of coronal brain sections shows expression of Fos+ (brown) in hypothalamic nuclei (outlined) of LC/hM3Dq mice. Tissue was counterstained with Nissl (blue). Scale, 100 µm. LHA, lateral hypothalamus area. DMH, dorsal medial hypothalamus. VMH, ventral medial hypothalamus.

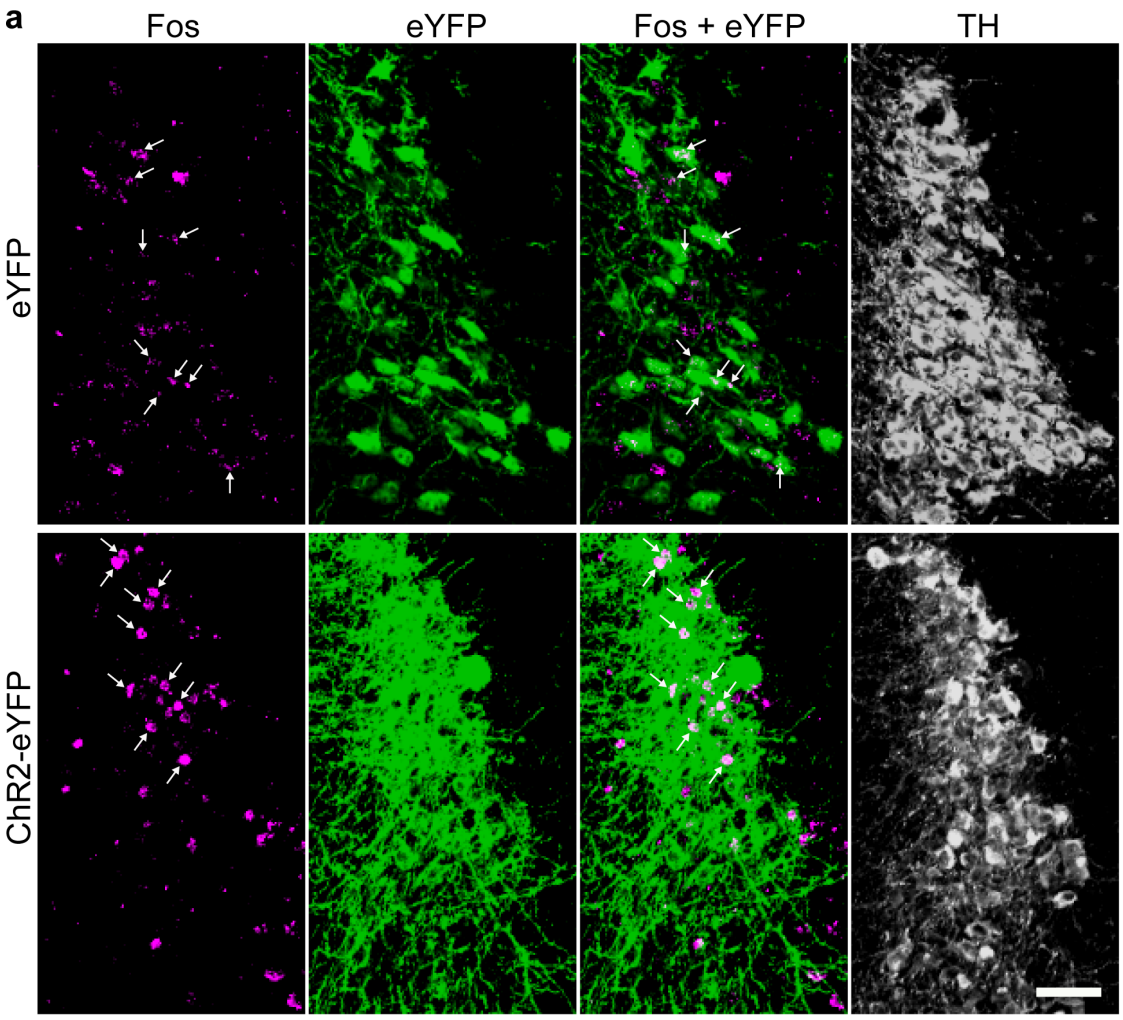
a
Fos
eYFP
Fos + eYFP
TH
eYFP
ChR2-eYFP

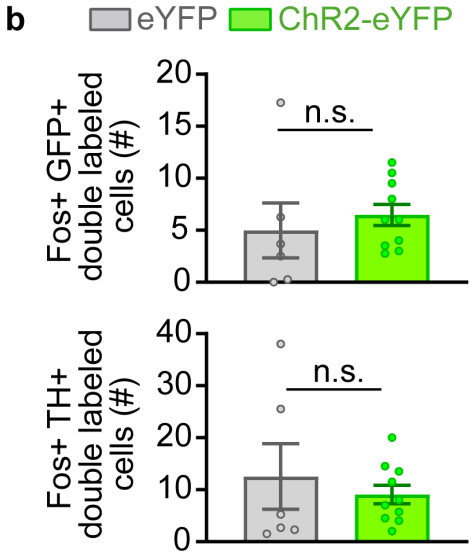
b
eYFP
ChR2-eYFP
Fos+ GFP+ double labeled cells (#)
20
15
10
5
0
n.s.
Fos+ TH+ double labeled cells (#)
40
30
20
10
0
n.s.

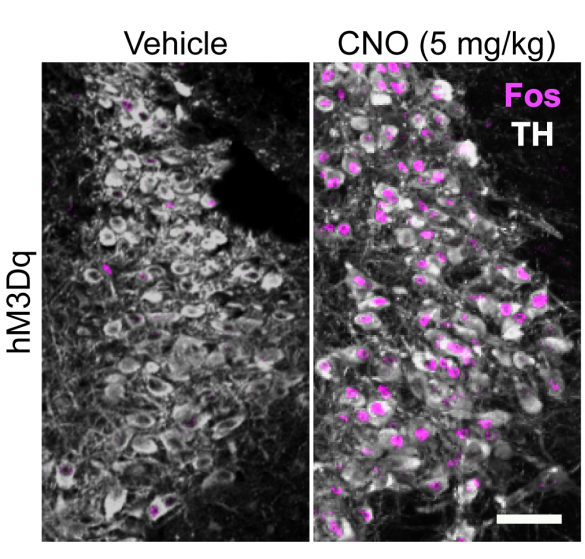
c
Vehicle
CNO (5 mg/kg)
hM3Dq
Fos
TH

Supplementary Figure 6. Stimulation of LC-LHA projection terminals does not influence somatic LC activity. (a) Immunofluorescent labeling of coronal brain sections shows co-expression of Fos+ (magenta) and eYFP+ (green) in noradrenergic (TH+, white) locus coeruleus neurons of $ChR2^{LC\text{-}LHA}$ mice and eYFP controls. Arrows indicate location of double-labeled Fos+ YFP+ neurons in the locus coeruleus. Scale, 50-μm. **(b)** *Top.* Double-labeled Fos+ YFP+ neurons in the locus coeruleus. Unpaired t-test: t_{14}=0.6213, P=0.5444. n=6 eYFP mice, n=10 ChR2 mice. *Bottom.* Double-labeled Fos+ TH+ neurons in the locus coeruleus. Unpaired t-test: t_{14}=0.6528, P=0.5244. n=6 eYFP mice, n=10 ChR2 mice. n.s., non-significant. **(c)** Immunofluorescent labeling of coronal brain sections shows co-expression of Fos+ (magenta) in noradrenergic (TH+, white) locus coeruleus neurons of vehicle-treated (negative control) and CNO-treated (positive control) LC^{hM3Dq} mice, confirming our ability to detect Fos expression. Scale, 50-μm.

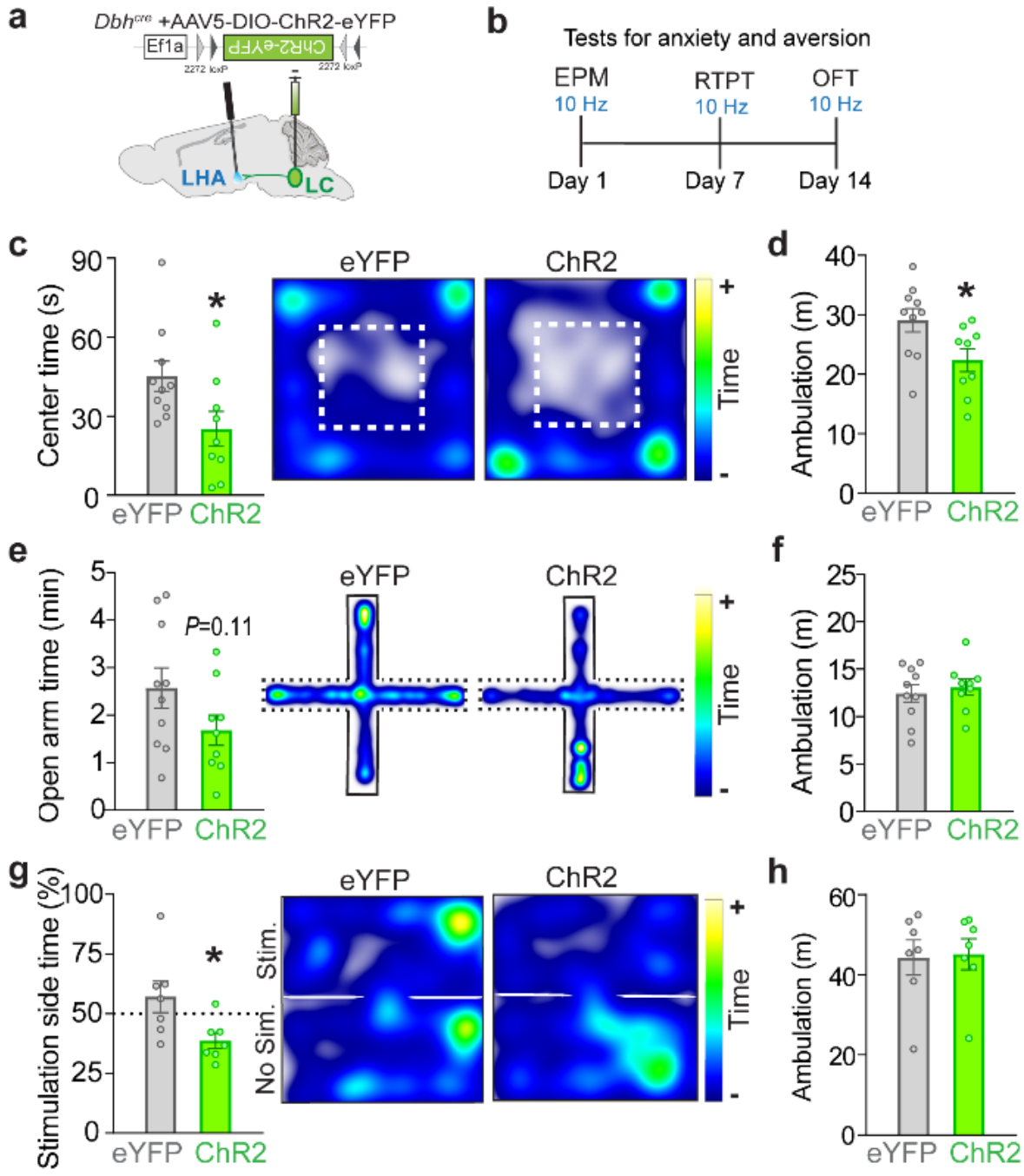

Supplementary Figure 7. Optogenetic stimulation of LC-LHA circuit is aversive and increases anxiety-like behavior. (a) Schematic shows viral and fiber optic delivery. **(b)** Timeline of anxiety and aversion tests, including the open field (OFT), elevated plus maze (EPM), and real time place test (RTPT). **(c-d)** OFT behaviors. Unpaired samples t-test: center time (**c**: t_{17}=2.279, P=0.0358) and ambulation (**d**, t_{17}=2.411, P=0.0275). **(e-f)** EPM behaviors. Unpaired samples t-

test: open arm time (**e**: t_{17}=1.638, P=0.1199) and ambulation (**f**, t_{17}=0.5101, P=0.6165). n=10 eYFP$^{LC\text{-}LHA}$ mice, n=9 ChR2$^{LC\text{-}LHA}$ mice. **(e-f)** RTPT behaviors. Unpaired samples t-test: stimulation side time (**e**: t_{12}=2.498, P=0.0280) and ambulation (**f**, t_{12}=0.1369, P=0.8934). n=7 eYFP$^{LC\text{-}LHA}$ mice, n=7 ChR2$^{LC\text{-}LHA}$ mice. Data are mean ± SEM. Representative spatial location heatmaps show the time spent exploring the arena.

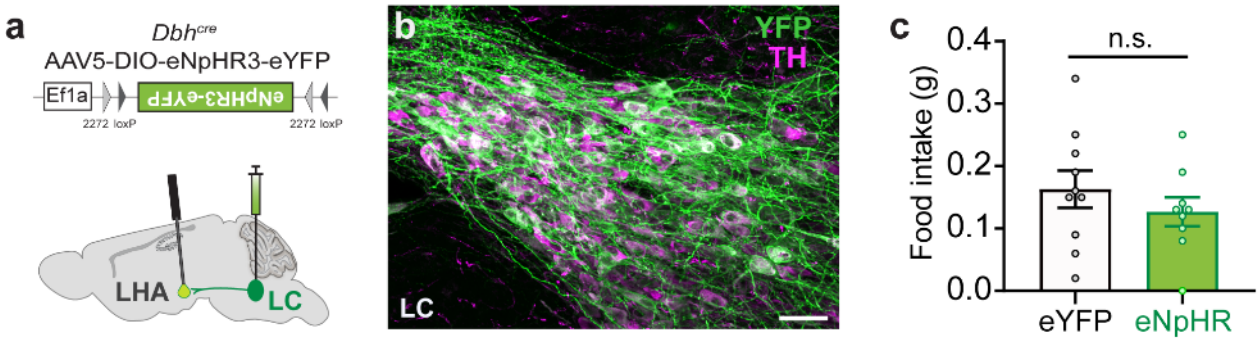

Supplementary Figure 8. Inhibition of LC-LHA circuit does not alter spontaneous food intake. **(a)** Schematic representation of sagittal mouse brain shows location of cre-dependent AAV used to drive eNpHR3.0-eYFP expression and location of fiberoptic probes. **(b)** Parasagittal section from eNpHR$^{LC\text{-}LHA}$ brain reveals eNpHR3.0-eYFP expression in LC-NE neurons. Scale, 50-μm. **(c)** Food intake measured for 30-min in free-feeding mice during photostimulation. Unpaired t-test: t_{17}=0.9491, P=0.3559. Data are mean ± SEM. n=10 eYFP mice, n=9 eNpHR$^{LC\text{-}LHA}$ mice.

METHODS

Animals

All procedures related to the use of animals were approved by the NIEHS Animal Care and Use Committee and were in accordance with the National Institutes of Health guidelines for the care and use of laboratory animals. Male and female mice that were >2 months of age were used for all studies. Mice were maintained on a reverse 12:12-hr light:dark cycle with lights off at 8 AM. All experiments occurred during the dark period of the circadian cycle. Mice had *ad libitum* access to water and standard food (NIH-31, Harlan, Madison WI), except when mice underwent 24-hr food-deprivation before the food intake test. Mice were group housed, unless surgical implants required singe housing.

Breeding

En1^{cre} [1], *Dbh*^{Flpo} [2], *RC::FL-hM3Dq*[3], *Dbh*^{cre} (manuscript submitted), and *Dbh*^{cKO} (unpublished reagent) mouse colonies are maintained on a C57BL/6J background. Triple transgenic mice were created by crossing *En1*^{cre} to double transgenic *Dbh*^{Flpo}*; RC::FL-hM3Dq* mice.

Tissue collection

Adult mice were deeply anesthetized with sodium pentobarbital and perfused transcardially with PBS followed by 4% PFA. Brains were postfixed overnight by immersion in 4% PFA at 4°C. Following rinse in PBS, tissue was cryoprotected in 30% sucrose in PBS and embedded in Tissue Freezing Medium (General Data Healthcare). 40-µm free-floating coronal or sagittal brain sections were collected in PBS, transferred to a cryoprotectant and stored at -80°C.

Immunohistochemistry

For immunofluorescence staining, mCherry-expressing neurons were detected using Rat anti-mCherry primary antibody (1:1000) and Goat anti-rat Alexa Fluor 568 secondary antibody (1:1000). eGFP and eYFP-expressing neurons and axons were detected using Chicken anti-GFP primary antibody (1:10,000 for free-floating tissue) and Goat anti-chicken Alexa Fluor 488 secondary antibody (1:1000). td-tomato+ neurons were detected using Rabbit anti-dsRed primary antibody (1:1000) and Goat anti-rabbit Alexa Fluor 568 secondary antibody (1:1000). The noradrenergic identify of neurons was confirmed with Rabbit anti-TH primary antibody (1:1000) and either Goat anti-rabbit 633 or Goat anti-rabbit 488 secondary antibody (1:1000). Mouse anti-TH primary antibody (1:500) was also used with either Goat anti-mouse 568 or Goat anti-mouse 633 secondary antibody (1:1000). For immunofluorescent staining, Fos was labeled with Rabbit anti-cFos primary antibody (1:250, Santa Cruz, sc-52) and Goat anti-Rabbit 633 secondary antibody (1:1000). NeuroTrace 435/455 blue fluorescent Nissl stain (1:50, N21479, ThermoFisher) was used to visualize neurons. For immunoperoxidase staining, Fos was detected using Rabbit anti-cFos primary antibody (1:2000, ab190289, Abcam) and biotinylated Goat anti-rabbit secondary antibody (1:500, BA-1000, Vector Labs) in conjunction with Vectastain Elite ABC kit and DAB substrate kit (Vector Labs). *In situ* hybridization was performed according to the manufacturer's instructions using a Fast red RNAscope probe that was targeted against Dbh (Mm-Dbh-O; 464621; Advanced Cell Diagnostics, Newark CA). Coverslips were applied using Vectashield hard-set mounting medium with or without DAPI (H-1500 or H-1400, Vector Labs) or Prolong Diamond Anti-Fade mounting medium (P36970, Invitrogen). Methods were performed as previously described[2,3]. The antibodies and riboprobes used are summarized below.

Antibody	Species	Dilution	Source	Catalog #	LOT #
mCherry	Rat	1:1000	Kerafast	EST202	105499
eGFP	Chicken	1:10,000 1:1000	Abcam	AB13970	236651-15
dsRed	Rabbit	1:1000	Clontech	632496	1612022
TH	Rabbit	1:1000	Millipore	AB152	2493925
TH	Mouse	1:500	GeneTex	GTX10372	821901979
c-Fos	Rabbit	1:250	Santa Cruz	Sc-52	K1115
c-Fos	Rabbit	1:2000	Abcam	ab190289	GR289729-1
Alexa Fluor 568 anti-rat	Goat	1:1000	Invitrogen	A-11077	1853640
Alexa Fluor 488 anti-chicken	Goat	1:1000	Invitrogen	A-11039	1812246
Alexa Fluor 488 anti-rabbit	Goat	1:1000	Invitrogen	A-11034	1812166
Alexa Fluor 568 anti-rabbit	Goat	1:1000	Invitrogen	A-11036	1924788
Alexa Fluor 633 anti-rabbit	Goat	1:1000	Invitrogen	A-21071	A21071
Alexa Fluor 633 anti-mouse	Goat	1:1000	Invitrogen	A-21052	1906490
Alexa Fluor 568 anti-mouse	Goat	1:1000	Invitrogen	A-11031	685228
Biotinylated anti-rabbit	Goat	1:500	Vector Labs	BA-1000	ZB0318

Riboprobe	Species	Source	Catalog #	LOT #
Dbh-O1	Mouse	Advanced Cell Diagnostics	464621	16180A

Digital image processing

Images of immunofluorescent-labeled sections were collected using a Zeiss LSM780 or 880 inverted confocal microscopes (Carl Zeiss Inc., Oberkochen, Germany). When necessary, Zen Black 2012 Software (Carl Zeiss) was used to convert z-stacks to maximum intensity projections. Images were modified only by adjusting brightness and contrast across the entire image to optimize the fluorescence signal. Anatomical location was confirmed by reference to a mouse brain atlas[4].

To measure Fos in LC-NE neurons, images of fluorescently-stained sections were acquired at 20x using a Zeiss LSM780 and digital images were subsequently exported to

MetaMorph (Molecular Devices, San Jose, CA). To measure Fos in the hypothalamus, brightfield images of DAB-stained brain sections were acquired at 40x using an Aperio AT2 slide scanner (Leica Biosystems Inc., Buffalo Grove, IL). Digital images were subsequently exported from Aperio Imagescope (Leica Biosystems) as an uncompressed *.tif file and opened in FIJI software v2 (http://imagej.net/Citing) for further analysis.

Cell counts

To measure Fos in LC-NE neurons, quantification was performed on every fourth 40-µm coronal section in the locus coeruleus and included at least 2-4 sections. An experimenter blind to treatment group performed the quantification. MetaMorph software was used to manually select TH+ and GFP+ cells individually, and then we used the automated count nuclei feature to identify Fos cells using the following settings: approximate minimum width was 6-µm and maximum width was 9-µm with intensity above background of 10 gray levels. To determine colocalization, the AND operation was used within the Arithmetic process to count colocalized pixels that were ≥ than 20 µm²; this size was large enough to ignore background noise but small enough to count overlap of individual cells. To confirm our ability to detect Fos expression, we used LC^{hM3Dq} mice treated with CNO (5 mg/kg i.p.) and vehicle; this control tissue was run in every immunohistochemistry assay.

To measure Fos in hypothalamic nuclei, quantification was performed on every fourth 40-µm coronal section in the lateral, dorsomedial, and ventromedial hypothalamus, and included at least 2-4 sections. An experimenter blind to treatment group performed the quantification. FIJI software was used to measure the region-of-interest and perform automated counting. The number of Fos+ neurons was normalized to mm^2 area.

Drugs

For behavioral studies, clozapine n-oxide (CNO, 5-mg/kg i.p., NIMH Drug Supply Program)[3] or yohimbine hydrochloride (3 mg/kg i.p., Tocris)[5-8] was administered by 20-min prior to testing. For study of fos expression, CNO (1-mg/kg i.p.) was administered 2 hours before perfusion. All compounds were injected at a volume of 0.1 mL/10 g body weight. Drugs were dissolved in DMSO (< 3%) and brought to volume using 0.9% physiological saline. For oral CNO administration, the doses selected were based on previously published papers (30 and 100 µg/mL)[9-12]. CNO water was prepared fresh daily by dissolving in 0.5% DMSO and brought to volume using reverse osmosis deionized (RODI) water.

Chemogenetic activation of LC-NE neurons during behavior

Food intake test (FI). To motivate feeding, mice were fasted a day prior to the food intake test[13]. Food-deprived mice were allowed 20-min to explore a two-compartment arena (25 x 25 x 25 cm) that contained two petri-dishes (60 x 15 mm) located on opposite corners. One dish contained standard food (NIH-31) and the other dish was empty. The dish location was randomly assigned and counterbalanced for each treatment group. For drug experiments, mice received CNO (5 mg/kg i.p.)[3] or vehicle approximately 20-min before the FI test. Ambulatory behavior was video recorded and analyzed using Ethovision versions 12-14 (Noldus, Leesburg VA). Food intake was recorded during the dark period of the circadian cycle by an experimenter blind to treatment. Mice were returned to *ad libitum* food after testing.

Labmaster feeding and metabolism. Mice were single-housed and allowed 4 days to acclimate to the Labmaster cages (23 x 13 x 1 cm) (TSE Systems, Bad Homburg, Germany). Following habituation, mice received water that contained vehicle or CNO (30 or 100 µg/mL) on alternate days, as used previously[9-12]. At the same circadian time each day (CT 10-11), food and water were replenished and mice were weighed by an experimenter. Food spillage was also monitored and measured by an experimenter, wherein large spillage events (>1g in 15-min) were

subtracted from total intake on rare occasions. *Ad libitum* food and drink was provided during the entire experiment. Measures of food and drink intake, and gas exchange were collected every 15-min. Meal number and size was measured using the sequence meal analysis setting, whereby all meals were recorded chronologically to evaluate single feeding episodes. Meals started when food consumption was greater than 0.02 g and ended when consumption ceased for at least 5-min [14,15]. For metabolic measures, O_2 and CO_2 were sampled for a 3-min period once every 15-min. Flow and sample rates were held at 0.3L/min and 0.25L/min respectively as determined by appropriate variation between the sample and reference cage. Respiratory exchange rate (RER) was derived by indirect calorimetry using the quotient VCO_2/VO_2. Energy expenditure (EE) was derived by the abbreviated Weir equation, $EE=(3.941*VO_2) + (1.106*VCO_2)$. Metabolic values were normalized to the daily body weights (metabolic values/body weight). Daily cumulative intake and averages of gas exchange were assessed for each 24-hr drug-dosing day. Circadian data were summarized over three periods: early lights OFF (ZT11-20), lights ON (ZT20-8), and late lights OFF (ZT8-10). Data were collected using the Labmaster version 2.6.9.13409 (TSE Systems) and analyzed by an experimenter blind to treatment.

Viral preparation

We generated a Flp-dependent GCaMP6f AAV construct for photometry experiments. pAAV-Ef1a-fDIO-EYFP (Addgene #55641) was digested with *Asc*I and *Nhe*I to remove the EYFP cDNA, and GCaMP6f cDNA was obtained from pGP-CMV-GCaMP6f (Addgene #40755)[16] digested with *Not*I and *Bgl*II restriction enzymes. After incompatible single-strand overhangs were filled-in to generate blunt ends, the two restriction fragments were ligated to produce plasmid pAAV-Ef1a-fDIO-GCaMP6f. DNA was packaged into an AAV5 serotyped virus by the NIEHS Viral Vector core. To generate pAAV-Ef1a-fDIO-tdTomato, a tdTomato cDNA was isolated from pRSET-tdTomato (generously provided by Roger Tsien) and cloned into pAAV-Ef1a EYFP digested with *Asc*I and *Nhe*I. The viruses and titers that were used are summarized below.

Plasmid	Virus source	Packaging	Serotype	Titer
pAAV-Ef1a-fDIO-GCaMP6f (addgene ID 128315)	Jensen lab (NIEHS)	NIEHS Viral Vector core	AAV5	1.44 x 10^{14} vg mL^{-1}
pAAV-Ef1a-fDIO-tdTomato (addgene ID 128434)	Jensen lab (NIEHS)	NIEHS Viral Vector core	AAV5	6.46 x 10^{12} vg mL^{-1}
pAAV-Ef1a-DIO hChR2(H134R)-eYFP	Deisseroth lab (Stanford)	UNC Viral Vector core	AAV5	7 x 10^{12} vg mL^{-1}
pAAV-Ef1a-DIO eYFP	Deisseroth lab (Stanford)	UNC Viral Vector core	AAV5	4.4 x 10^{12} vg mL^{-1}
pAAV-Ef1a-DIO-eNpHR3.0-eYFP	Deisseroth lab (Stanford)	UNC Viral Vector core	AAV5	3.1x 10^{12} vg mL^{-1}

Surgery

Mice were anesthetized using 4% isoflurane and placed in a stereotaxic frame (Kopf Instruments, Model 900) equipped with a digital micromanipulator (Harvard Apparatus, Holliston, MA). Anesthesia was maintained with 0.5-2% isoflurane and/or a cocktail of ketamine/xylazine (100/7 mg/kg i.p.). Bupivicaine (270 µg in 0.1ml) was injected locally beneath the scalp prior to incision. For viral injections, 500-nL volume was delivered at the rate of 100-nL per min using a 30-gauge Neuros Hamilton syringe or 26-gauge needle attached to a microsyringe (7002, Hamilton, Reno NV) and pump (UMP3 UltraMicroPump, WPI, Sarasota FL). Needles were left in place for 5 minutes after infusion to minimize backflow of the virus upon withdrawal of the needle. To minimize post-operative pain, all mice received the analgesic Buprenorphine SR (1 mg kg^{-1} s.c.). Mice were given a minimum recovery time of 4 (for LC soma experiments) or 6 weeks (for LC fiber experiments) to allow sufficient time for viral infection, genetic recombination and gene expression before behavioral measurements.

Surgery for photometry experiments. The locus coeruleus of *Dbh*^{Flpo} mice were injected with a 1:5 viral cocktail of *Flp*-dependent GCaMP6f (AAV5-fEf1a-fDIO-GCaMP6f) and tdTomato (AAV5-Ef1a-fDIO-tdTomato) using the following stereotaxic coordinates: −5.45 posterior; +/- 1.0 lateral; -3.75 ventral (mm from bregma). For experiments combining chemogenetics with photometry, both triple transgenic *En1*^{cre}*; Dbh*^{Flpo}*; R/C::FL-hM3Dq* (LC^{hM3Dq}) and double

transgenic *Dbh^{Flpo}; R/C::FL-hM3Dq* (LC^{GFP}) mice were used. The locus coeruleus of LC^{hM3Dq} mice were injected with a Flp-dependent GCaMP6f AAV and a subset of these mice were also co-injected with a Flp-dependent tdTomato AAV at least 3 weeks before optical probe implantation. All mice were unilaterally implanted with optical probes above the LC (-5.45 posterior, ±0.85 lateral, -3.71 to -4.31 ventral, mm from bregma). Optical probes (multimode optical fibers: 200-µm core with 0.39 NA or 105 µm core with 0.22 NA, Thor Labs) were adhered within a ceramic ferrule (1.25-mm OD, Precision Fiber Products, Inc.) with epoxy (PFP 353ND, Precision Fiber Products, Inc.). Final placement of the probe was guided by live fluorescence signal as described below (see *Photometry Recordings* section). Optical probes were anchored to the skull using 3 skull screws, Metabond, and dental acrylic.

Surgery for optogenetic experiments. *Dbh^{cre}* mice received bilateral LC injections of the cre-dependent virus encoding ChR2-eYFP (AAV5-Ef1a-DIO-ChR2-eYFP), eNpHR (AAV5-Ef1a-DIO-eNpHR3.0-eYFP) or eYFP control (AAV-Ef1a-DIO-eYFP) using the following coordinates: -5.45 posterior, ±1.28 lateral, -3.65 mm ventral (mm from bregma)[17]. During the same surgery, mice were implanted with bilateral fiber-optic cannula (MFC_200/250-0.66_5mm_ZF1.25_FLT, Doric Lenses Inc., Quebec Canada) angled 10° over the LHA using the following coordinates: -1.70 posterior, ±1.71 lateral, -4.82 ventral (mm from bregma)[13]. The implants were secured using Metabond (Parkel, Edgewood NY) and dental acrylic (Lang Dental Manufacturing Co. Inc., Wheeling IL). It is important to note that we performed histology on every mouse to verify expression of virus and fiber placement. For behavioral experiments, only the mice that had selective expression of ChR2, eNpHR or eYFP in TH+ locus coeruleus neurons, but no expression in other TH+ noradrenergic nuclei (e.g., A1, A2, A5), were included for analysis.

LC-NE photometry recordings

In vivo optical recording of GCaMP6f, tdTomato and GFP fluorescent intensities were measured in LC-NE neurons using a custom-built fiber photometry system, as previously

described[18,19]. Excitation light (488 nm, 20 mW continuous wave laser, OBIS 488LS-20, Coherent, Inc.) was collected by multimode patch cables (M61L01: 105-µm core with 0.22 NA; M72L05, 200-µm core with 0.39 NA, Thor Labs) and passed through a fluorescent cube (DFM1, Thor Labs) containing an excitation filter (59004x, Chroma) and dichroic mirror (ZT488/561rpc-UF1, Chroma). Excitation light was then reflected into an achromatic fiber port (PAFA-X-4-A, Thor Labs) and patch cable linked to an implantable ferrule containing the optical fiber and ceramic sleeve (SM-CS125S, Precision Fiber Products Inc.). Excitation light from the implantable fiber was adjusted to 70-µW. Using the same optical fiber and patch cable, emitted light was passed through a dichroic mirror and emission filter (ZET 488/561m) before collection by a multi-mode patch cable (M200L02-A, 0.39 NA, AR-coated 200/230 µm core/cladding, Thor Labs). Emitted light was then collected into a spectrometer (QE Pro-FL, Ocean Optics, Inc.) and visualized using Ocean View version 1.5. The spectrometer and camera (Basler, acA1300-60gm) were triggered using a Doric TTL pulse generator (OTPG_4, Neuroscience Studio Software, Doric Lenses, Inc., Quebec, Canada). Mice were given 1-week for surgical recovery and then were habituated for several days (20-min/day) to being tethered to optical patch cables while in the testing arena (30 x 30 x 35.5 cm, Phenotyper, Noldus Information Technology, Inc., Leesburg, VA, USA). All photometry recordings occurred during the dark phase of the circadian light:dark cycle.

Photometry recordings for sensory experiments. A 1-s flash of light was presented every minute during the recording session which lasted ~30-min. The light source (Dual Channel Optogenetics-Lime-Green-LED module, Prismatix, Givat-Shmuel, Israel) was connected to a polymer optical fiber (500-µm, NA 0.63, Prismatix) that was positioned indirectly above the testing arena (Phenotyper).

Photometry recordings for feeding experiments. Prior to recordings, mice were habituated for several days to eating from the feeding experimentation device (FED)[20] in both the homecage and testing arena (Phenotyper). The FED dispensed grain-based chow (25-mg pellets, Test Diet 5TUM) with a 60-s delay after retrieval of each pellet. This delay was used to space out

pellets, which facilitated analysis of consumption responses during LC calcium recordings in overnight fasted mice. Recordings collected with the FED lasted 60-min.

Photometry recordings for pharmacology studies. Recordings lasted 35-min including 15-min prior to injection and 20-min post-injection. In all experiments, data were collected at 25-Hz from the camera and spectrometer (and FED when appropriate) and were synchronized using Ethovision (Noldus).

Photometry data analysis

GCaMP6f and tdTomato fluorescent intensity (F) were calculated as the sum of intensity values between 500-540 nm and 575-650 nm, respectively, for each frame. Linear unmixing was performed to separate fluorescent overlap between GCaMP6 and tdTomato emission spectra as described previously[18]. To control for movement artifact in fluorescent signal, the unmixed GCaMP coefficients were normalized to unmixed tdTomato coefficients to yield a fluorescent ratio value.

Analysis of LC recordings during feeding and visual events. We used RStudio (64-bit version 1.2.1335, RStudio, Inc., Boston, MA, USA) to run custom computer code (see *Code Availability* section) to align fluorescent ratio signals to relevant experimental events (i.e., pellet retrieval for feeding experiments, light flash for sensory experiments). The fluorescent ratio signal was assessed independently for each event around a 90-s window. Each fluorescent ratio value was transformed into a z-score by subtracting the mean of a baseline period (45-30 s before retrieval) and dividing the SD of the baseline period. For feeding experiments, the 90-second window was divided into four behavioral windows: baseline (45-30 s before pellet retrieval), approach (1-s before pellet retrieval), consumption (1-6 s after pellet retrieval) and post-consumption (30-45 s after pellet retrieval). Analysis periods were selected based on visual observation of behavior (see **Supplemental Fig. 3a)**. To assess if LC activity varies as mice approached satiety, we compared LC responses during approach and consumption during the

first and last ten pellets of the recording session. Additionally, baseline activity for the first and last ten pellets of the recording session was calculated as a percentage of average GCaMP6f/tdTomato ratio during the ten-pellet bins normalized to GCaMP/tdTomato ratio during a 15-sec baseline window prior to the first pellet consumption.

For visual experiments, the 90-second window was divided into three behavioral windows: pre-light (45-30 s before light onset), light (1-s), and post-light (30-45 s after light onset). An average of the z-scores within the behavioral windows were reported and then averaged across events for each subject. Perievent Raster's and associated example traces were plotted using Neuroexplorer 5.109 (64-bit version). All other traces were plotted using GraphPad Prism 7 or 8 (GraphPad Software Inc., La Jolla CA).

Analysis of LC recordings during drug experiments. For quantification of pharmacological effects (in Fig. 2b, bottom trace), the average z-score fluorescent ratio was averaged across 5-min bins and the frames collected while the experimenter was present for mouse drug injection was excluded from these bins. Using the manual scoring feature in Ethovision 14, an experimenter blind to treatment condition separately marked each experimental video file for precise timeframes in which the **(1) experimenter was first present** and **(2) experimenter was first absent** from the sound-attenuating curtain which enclosed the testing arena. "Experimenter first present" was defined as the first video frame in which the door of the sound-attenuating curtained area opened (which increased darkened pixels in the video file) reliably and immediately before the experimenter entered. "Experimenter first absent" was defined as the first video frame in which the door of the sound-attenuating curtain was closed for experimenter's exit.

Optogenetic stimulation of LC-LHA circuit during feeding and anxiety-related behaviors

$ChR2^{LC\text{-}LHA}$ mice and eYFP controls were briefly anesthetized (4% isoflurane) to connect the fiber-optic cannula to bilateral optical cables (0.48 NA cable measuring 0.5-, 0.6- or 1-meter

in length with LC ferrule, BFP(2)_200/300/900-0.48_FCM-2xMF1.25). While in the homecage, mice were given 20-min to recover before optical stimulation. For stimulation of LC fibers, mice received 10-Hz (10-ms pulse width) photostimulation (6-9 mW total power) using the Doric system (LEDFRJ 465 nm powered by LEDD driver, Neuroscience Studio Software, Doric Lenses), as previously described[17,21]. Behavior was video-recorded using a Basler (acA1300-60gm) or Logitech (C930e) camera and analyzed by an experimenter blind to treatment group. All experiments were performed during the dark period of the circadian cycle.

Food intake test (FI). All mice were habituated to being tethered in the testing arena (20 x 20 x 25 cm) for 20-min on a day prior to testing. Mice were tested in a 30-min session while receiving photostimulation (10-Hz, 10-ms pulse width). For epoch experiments, mice were tested in a 30-min session consisting of 10-min photostimulation ON-1, 10-min photostimulation OFF, and 10 min photostimulation ON-2. Food intake was recorded by an experimenter blind to treatment.

Elevated plus maze (EPM). Mice were placed in a '+' shaped maze (Stoelting Co), as previously described[3]. The maze had two open (35 x 5 cm, 15 mm lip) and two closed arms (35 x 5 x 15 cm) and was elevated 50-cm. Mice could explore for 5-min while receiving photostimulation (10-Hz, 10-ms pulse width). The time spent in the open arms was recorded using Ethovision v12-14.

Real-time place test (RTPT). Mice were allowed 20-min to explore an unbiased two-compartment arena (50 x 50 x 25 cm), as described previously[13,17]. Photostimulation (10-Hz, 10-ms pulse width) occurred upon entry into one compartment and persisted until the mouse exited the compartment. The stimulation compartment was randomly assigned and counterbalanced for each treatment group. The percentage of time spent in the photostimulation-paired compartment was recorded by Ethovision v12-14.

Open field test (OFT). Mice were given 10-min to explore a clear plexiglass arena (45 x 45 x 30 cm) while they received photostimulation (10-Hz, 10-ms pulse width)[3]. The time spent in the center of the arena was recorded using Ethovision v12-14.

Optogenetic inhibition of LC-LHA circuit during feeding

eNpHR$^{LC\text{-}LHA}$ mice and eYFP controls were briefly anesthetized (4% isoflurane) to connect the fiber-optic cannula to bilateral polymer optical fibers (0.63 NA, 500-µm core diameter, 0.5-meter length, FC/PC connector, Prismatix), connected to an output port of a fiber optic rotary joint (Prizmatix). Mice were given 20-min to recover in the homecage before testing. During the food intake test (see *FI section* above for test details), mice received constant Lime-Green LED illumination (5-mW total power, Dual Channel Optogenetics-Lime-Green-LED module, Prismatix). Food intake was measured for 30-min in free-feeding mice by an experimenter blind to treatment group. All experiments occurred during the dark period of the circadian cycle.

Statistical analysis

All data are expressed as mean ± standard error (SEM). t-tests and ANOVAs were used to determine differences between groups. Bonferroni posthoc tests were used as appropriate. Significance was set at $P<0.05$. for all analyses. All predictions were two-tailed unless otherwise stated to assess *a priori* predictions. For quantification of Fos expression following LC^{hM3Dq} activation, we used one-tailed tests to assess a *priori* predictions. Analyses were conducted using GraphPad Prism 7 or 8 (GraphPad Software Inc.) and IBM SPSS software for Windows, version 21 (SPSS Inc., Chicago IL). Statistics and sample size are listed in the figure legends.

Code Availability

We deposited the custom computer code (R, 64-bit version 3.5.1) we used to align fluorescent ratio signals to the open-source software platform Github. The code can be accessed using the following link: https://github.com/NIEHS/FED-and-Photometry-Data-Processing.

Reporting Summary

Further information on experimental design is available in the Nature Research Reporting Summary linked to this article.

Data and code availability

All data generated or analyzed during this study are included in this published article (and this supplementary information file).

REFERENCES

1 Li, J. Y., Lao, Z. & Joyner, A. L. Changing requirements for Gbx2 in development of the cerebellum and maintenance of the mid/hindbrain organizer. *Neuron* **36**, 31-43 (2002).

2 Robertson, S. D., Plummer, N. W., de Marchena, J. & Jensen, P. Developmental origins of central norepinephrine neuron diversity. *Nat Neurosci* **16**, 1016-1023, doi:10.1038/nn.3458 (2013).

3 Sciolino, N. R. *et al.* Recombinase-Dependent Mouse Lines for Chemogenetic Activation of Genetically Defined Cell Types. *Cell Rep* **15**, 2563-2573, doi:10.1016/j.celrep.2016.05.034 (2016).

4 Paxinos, G. & Franks, K. B. J. *The mouse brain in sterotaxic coordinates*. (Academic Press, 2013).

5 Callahan, M. F., Beales, M. & Oltmans, G. A. Yohimbine and rauwolscine reduce food intake of genetically obese (obob) and lean mice. *Pharmacol Biochem Behav* **20**, 591-599 (1984).

6 Currie, P. J. & Wilson, L. M. Yohimbine attenuates clonidine-induced feeding and macronutrient selection in genetically obese (ob/ob) mice. *Pharmacol Biochem Behav* **43**, 1039-1046 (1992).

7 Holmes, A., Yang, R. J. & Crawley, J. N. Evaluation of an anxiety-related phenotype in galanin overexpressing transgenic mice. *J Mol Neurosci* **18**, 151-165, doi:10.1385/JMN:18:1-2:151 (2002).

8 Nicolas, L. B., Kolb, Y. & Prinssen, E. P. A combined marble burying-locomotor activity test in mice: a practical screening test with sensitivity to different classes of anxiolytics

and antidepressants. *Eur J Pharmacol* **547**, 106-115, doi:10.1016/j.ejphar.2006.07.015 (2006).

9 Urban, D. J. *et al.* Elucidation of The Behavioral Program and Neuronal Network Encoded by Dorsal Raphe Serotonergic Neurons. *Neuropsychopharmacology* **41**, 1404-1415, doi:10.1038/npp.2015.293 (2016).

10 Jain, S. *et al.* Chronic activation of a designer G(q)-coupled receptor improves beta cell function. *J Clin Invest* **123**, 1750-1762, doi:10.1172/JCI66432 (2013).

11 Cassataro, D. *et al.* Reverse pharmacogenetic modulation of the nucleus accumbens reduces ethanol consumption in a limited access paradigm. *Neuropsychopharmacology* **39**, 283-290, doi:10.1038/npp.2013.184 (2014).

12 Carvalho Poyraz, F. *et al.* Decreasing Striatopallidal Pathway Function Enhances Motivation by Energizing the Initiation of Goal-Directed Action. *J Neurosci* **36**, 5988-6001, doi:10.1523/JNEUROSCI.0444-16.2016 (2016).

13 Jennings, J. H., Rizzi, G., Stamatakis, A. M., Ung, R. L. & Stuber, G. D. The inhibitory circuit architecture of the lateral hypothalamus orchestrates feeding. *Science* **341**, 1517-1521, doi:10.1126/science.1241812 (2013).

14 Bake, T., Murphy, M., Morgan, D. G. & Mercer, J. G. Large, binge-type meals of high fat diet change feeding behaviour and entrain food anticipatory activity in mice. *Appetite* **77**, 60-71, doi:10.1016/j.appet.2014.02.020 (2014).

15 Stengel, A. *et al.* Activation of brain somatostatin 2 receptors stimulates feeding in mice: analysis of food intake microstructure. *Physiol Behav* **101**, 614-622, doi:10.1016/j.physbeh.2010.09.009 (2010).

16 Chen, T. W. *et al.* Ultrasensitive fluorescent proteins for imaging neuronal activity. *Nature* **499**, 295-300, doi:10.1038/nature12354 (2013).

17 McCall, J. G. *et al.* CRH Engagement of the Locus Coeruleus Noradrenergic System Mediates Stress-Induced Anxiety. *Neuron* **87**, 605-620, doi:10.1016/j.neuron.2015.07.002 (2015).

18 Meng, C. *et al.* Spectrally Resolved Fiber Photometry for Multi-component Analysis of Brain Circuits. *Neuron* **98**, 707-717 e704, doi:10.1016/j.neuron.2018.04.012 (2018).

19 Cui, G. *et al.* Deep brain optical measurements of cell type-specific neural activity in behaving mice. *Nat Protoc* **9**, 1213-1228, doi:10.1038/nprot.2014.080 (2014).

20 Nguyen, K. P., O'Neal, T. J., Bolonduro, O. A., White, E. & Kravitz, A. V. Feeding Experimentation Device (FED): A flexible open-source device for measuring feeding behavior. *J Neurosci Methods* **267**, 108-114, doi:10.1016/j.jneumeth.2016.04.003 (2016).

21 Uematsu, A. *et al.* Modular organization of the brainstem noradrenaline system coordinates opposing learning states. *Nat Neurosci* **20**, 1602-1611, doi:10.1038/nn.4642 (2017).